SAND REPORT
SAND2002-2519
Unlimited Release
Printed August 2002

Parametric Study for Large Wind Turbine Blades: WindPACT Blade System Design Studies

TPI Composites, Inc.
373 Market Street
Warren, RI 02885

Prepared by
Sandia National Laboratories
Albuquerque, New Mexico 87185 and Livermore, California 94550

Sandia is a multiprogram laboratory operated by Sandia Corporation, a Lockheed Martin Company, for the United States Department of Energy under Contract DE-AC04-94AL85000.

Sandia National Laboratories

Issued by Sandia National Laboratories, operated for the United States Department of Energy by Sandia Corporation.

Available to DOE and DOE contractors from
U.S. Department of Energy
Office of Scientific and Technical Information
P.O. Box 62
Oak Ridge, TN 37831

Telephone: (865)576-8401
Facsimile: (865)576-5728
E-Mail: reports@adonis.osti.gov
Online ordering: http://www.doe.gov/bridge

Available to the public from
U.S. Department of Commerce
National Technical Information Service
5285 Port Royal Rd
Springfield, VA 22161

Telephone: (800)553-6847
Facsimile: (703)605-6900
E-Mail: orders@ntis.fedworld.gov
Online order: http://www.ntis.gov/ordering.htm

SAND2002-2519
Unlimited Release
Printed August 2002

PARAMETRIC STUDY FOR LARGE WIND TURBINE BLADES

WindPACT Blade System Design Studies

TPI Composites, Inc.
373 Market Street
Warren, RI 02885

Abstract

This report presents the results of a study of various wind turbine blade design parameters as a function of blade length in the range from 30 meters to 70 meters. The results have been summarized in dimensional and non-dimensional formats to aid in interpretation. The parametric review estimated peak power and annual energy capture for megawatt scale wind turbines with rotors of 62, 83, 104, 125, and 146 meters in diameter. The baseline "thin" distribution represents conventional airfoils used in large wind turbine blades. The "thicker" and "thickest" distributions utilize airfoils that have significantly increased thickness to improve structural performance and reduce weight. An aerodynamic scaling effort was undertaken in parallel with the structural analysis work to evaluate the effect of extreme thickness on aerodynamic characteristics. Increased airfoil section thickness appears to be a key tool in limiting blade weight and cost growth with scale. Thickened and truncated trailing edges in the inboard region provide strong, positive effects on blade structural performance. Larger blades may require higher tip speeds combined with reduced blade solidity to limit growth of design loads. A slender blade can be used to reduce extreme design loads when the rotor is parked, but requires a higher tip speed.

Acknowledgements

TPI Staff: Derek Berry and Steve Lockard
Dynamic Design: Kevin Jackson
MDZ Consulting: Mike Zuteck
Cal Davis: Case Van Dam

Sandia Technical Monitor: Tom Ashwill

This is a Contractor Report for Sandia National Laboratories that partially fulfills the deliverables under Contract #15890.

TABLE OF CONTENTS

LIST OF FIGURES **6**
LIST OF TABLES **8**
SUMMARY **9**

1.0 ANALYSIS APPROACH **11**
1.1 Goals and Objectives 11
1.2 Blade Planform Definition 11
1.3 Performance Model 12
1.4 Blade Thickness Definition 15
1.5 Blade Structural Scaling 15
1.6 Blade Structural Analysis 17
1.7 Blade Design Loads 19
1.8 Blade Aerodynamic Scaling 21
1.9 Thick Airfoil Properties 23

2.0 STUDY RESULTS **24**
2.1 Performance Scaling Results 24
2.1.1 Rotor Performance Scaling 24
2.2 Structural Scaling Results 27
2.2.1 Blade Laminate Weight Scaling 27
2.2.2 Tip Deflection Scaling 30
2.2.3 Simplified Economic Scaling 30
2.3 Airfoil Scaling Results 35
2.3.1 Effect of Thickness on Aerodynamic Performance 35
2.3.2 Effect of Scaling Approach on Airfoil Performance 39
2.3.3 Effect of Trailing-Edge Thickness on Aerodynamic Performance 41

3.0 CONCLUSIONS **44**
3.1 Significant Findings 44
3.2 Recommendations for Further Study Resulting From This Study 44

4.0 REFERENCES **45**

LIST OF FIGURES

Figure 1.1 Drawing of Non-Dimensional Blade Planform 12

Figure 1.2 30 Meter Blade Power Curves for Various Tip Speeds 14

Figure 1.3 30 Meter Blade Thickness as Function of Radial Station for Three Thickness Variations 15

Figure 1.4 Illustration of Blade Sections at 15% Span 16

Figure 1.5 Illustration of Blade Sections at 25% Span 16

Figure 1.6 Illustration of Blade Sections at 45% Span 17

Figure 1.7 Typical Blade Construction 17

Figure 1.8 Comparison of 30m Blade Loads for Two Analysis Approaches 20

Figure 1.9 Aerodynamically Scaled Airfoil Thickness Distribution 22

Figure 1.10 Comparison of Airfoil Shapes Developed Using Structural and Aerodynamic Scaling Methods 22

Figure 1.11 Closeup of Streamline Grid About S821 Airfoil for Converged Solution at α = 10.0°, Re = 2.30 million, M_8 = 0.1, Free Transition 23

Figure 2.1 Peak Power as a Function of Rotor Diameter and Tip Speed 24

Figure 2.2 Contour Plot of Energy Production as a Function of Diameter and Tip Speed for a 5.5 m/s Mean Rayleigh Wind Distribution 26

Figure 2.3 Contour Plot of Energy Production as a Function of Diameter and Tip Speed for a 6.0 m/s Mean Rayleigh Wind Distribution 26

Figure 2.4 Contour Plot of Energy Production as a Function of Diameter and Tip Speed for a 6.5 m/s Mean Rayleigh Wind Distribution 27

Figure 2.5 Blade Laminate Weight as a Function of Rotor Diameter 28

Figure 2.6 Contour Plot of Blade Laminate Weight as a Function of Section Thickness and Rotor Diameter 29

Figure 2.7 Blade Specific Weight as a Function of Rotor Diameter 29

Figure 2.8 Contour Plot of Blade Specific Weight 30

Figure 2.9 Blade Tip Deflection as a Function of Rotor Diameter 31

Figure 2.10 Contour Plot of Tip Deflection as a Function of Rotor Diameter 32

Figure 2.11 Specific Tip Deflection as a Function of Rotor Diameter 32

Figure 2.12 Contour Plot of Specific Deflection 33

Figure 2.13 Contour Plot of Rotor Cost Scaling 34

Figure 2.14 Contour Plot of Energy Sales Scaling 34

Figure 2.15 Contour Plot of Simple Rotor Payback Scaling 35

Figure 2.16 Lift Characteristics of S821 Airfoil at Re = 2.30 million and Re = 4.35 million, Free and Fixed Transition 36

Figure 2.17 Thickness Effect on Lift at Re = 2.30 million, Free and Fixed Transition 37

Figure 2.18 Thickness Effect on Lift at Re = 4.35 million, Free and Fixed Transition 38

Figure 2.19 Thickness Effect on L/D at Re = 2.30 million, Free and Fixed Transition 38

Figure 2.20 Thickness Effect on L/D at Re = 4.35 million, Free and Fixed Transition 39

Figure 2.21 Comparison of S821-38 Airfoil and Station 25% 38% t/c Airfoil Obtained Through XY Scaling 40

Figure 2.22 Effect of Airfoil shape on Lift and Lift-to-Drag Ratio at Re = 4.35 million, Free and Fixed Transition 40

Figure 2.23 Effect of Airfoil Shape on Lift-to-Drag Ratio at Re = 4.35 million, Free and Fixed Transition 41

Figure 2.23 Comparison of Sharp-Trailing-Edge Airfoil S821-38 and Airfoil S821-38-02 With Trailing-Edge Thickness of 2.0% 42

Figure 2.24 Effect of Trailing-Edge Thickness Shape on Airfoil Lift at Re = 4.35 million, Free and Fixed Transition 43

Figure 2.25 Effect of Trailing-Edge Thickness Shape on Airfoil Lift-to-Drag Ratio at Re = 4.35 million, Free and Fixed Transition 43

LIST OF TABLES

Table 1.1 Non-Dimensional Blade Planform Definition 11
Table 1.2 Turbine Rotor Characteristics 12
Table 1.3 Non-Dimensional Rotor Performance 13
Table 1.4 Turbine Rotational Speeds 13
Table 1.5 Turbine Component Power Ratings 13
Table 1.6 Non-Dimensional Gearbox Efficiency 14
Table 1.7 Non-Dimensional Generator Efficiency 14
Table 1.8 Non-Dimensional Blade Thickness Distribution 15
Table 1.9 Summary of Structural Details 18
Table 1.10 Non-Dimensional Blade Thickness Distribution 19
Table 1.11 30 m Blade Extreme Moment Loading Results 20
Table 2.1 Performance as a Function of Rotor Diameter and Tip Speed 25
Table 2.2 Specific Production as a Function of Rotor Diameter and Tip Speed 25
Table 2.3 Blade Laminate Weight as a Function of Rotor Diameter 28
Table 2.4 Blade Tip Deflection as a Function of Rotor Diameter 31
Table 2.5 Simplified Economic Scaling Parameters 33
Table 2.6 Aerodynamic Performance Characteristics of the S821 Airfoil 36

SUMMARY

This report presents the results of a study of various wind turbine blade design parameters as a function of blade length in the range from 30 meters to 70 meters. The results have been summarized in dimensional and non-dimensional formats to aid in interpretation.

The parametric review estimated peak power and annual energy capture for megawatt scale wind turbines with rotors of 62, 83, 104, 125, and 146 meters in diameter. The annual energy production for each rotor size was evaluated as a function of tip speed at 60, 65, and 70 m/s, which brackets the operating range of typical commercial wind turbines. The analysis assumed a Rayleigh wind distribution and did not include losses due to availability, arrays, air density variation, blade soiling, control systems, or electrical distribution

The baseline "thin" distribution represents conventional airfoils used in large wind turbine blades. The "thicker" and "thickest" distributions utilize airfoils that have significantly increased thickness to improve structural performance and reduce weight. The blade cross-section structural characteristics were estimated at five spanwise locations (15%, 25%, 45%, 65%, and 85% of radius). The blade construction was assumed to be a stressed shell.

The aerodynamic properties of the thick airfoils assumed in the structural analysis were not available from the literature. As a result it was necessary to estimate the aerodynamic characteristics of the thick airfoil sections. An aerodynamic scaling effort was undertaken in parallel with the structural analysis work to evaluate the effect of extreme thickness on aerodynamic characteristics.

The NREL S821 was selected as the baseline airfoil used in the aerodynamic scaling study. A series of scaled airfoil versions were developed and analyzed. The maximum thickness-to-chord ratio (t/c) was modified in increments of approximately 5%, starting at 24% for the S821 and ending with an extreme design case of 60% t/c.

In the blade range from 30 to 70 meters the blade weight grew as the cube of the length for all three cross-sections studied. The economic performance of the blades is inversely related to the specific weight, defined as the blade weight divided by capture area (kg/m^2), which more than doubled over the same range. A number of design changes will be required to limit cost growth. No one technology can stop weight growth, but it can be limited by a number of design approaches.

Increased airfoil section thickness appears to be a key tool in limiting blade weight and cost growth with scale. Thickened and truncated trailing edges in the inboard region provide strong, positive effects on blade structural performance. From the thin to thickest blade distribution the specific weight was reduced by 15%, due to increased structural performance.

The results show a beneficial influence of trailing-edge thickness on the lift-curve slope as well as the maximum lift coefficient on high thickness airfoil sections. The problem with thick (t/c > 26%) airfoils is that their lift performance is sensitive to changes in the boundary layer location (i.e. the lift at fixed angle of attack decreases as a result of a forward shift in transition due to surface fouling). This sensitivity to premature transition is reduced by increasing trailing edge thickness.

Larger blades may require higher tip speeds combined with reduced blade solidity to limit growth of design loads. A slender blade can be used to reduce extreme design loads when the rotor is parked, but requires a higher tip speed. Noise issues become a concern with higher tip speeds. Blade tip speed can strongly impact peak power. Increasing tip speed was found to exhibit a relatively weak, but positive influence on annual energy capture.

1.0 ANALYSIS APPROACH

1.1 Goals and Objectives

The primary goal of the WindPACT Blade System Design Study (BSDS) was investigation and evaluation of design and manufacturing issues for wind turbine blades in the megawatt size range. The results of the initial engineering study will guide design specifications and preliminary engineering for candidate blades in the range of 30 to 70 meters in length. Subsequent efforts will generate detailed recommendations for sub-scale and sub-structure testing that will help determine the feasibility of innovations and provide data for detailed design in follow-on contracts.

The initial project task, described in this report, was to assess the fundamental physical and manufacturing issues that govern and constrain large blades. The Issues and Constraints phase of the project entails three basic elements: 1) a Parametric Scaling Study to assess blade structure using current technology, 2)a Current Fabrication Technology evaluation of the cost to manufacture, transport, and install large blades, and 3) identification of promising Innovative Design Approaches that show potential for overcoming fundamental physical and manufacturing constraints.

This report discusses the approach used to perform the parametric scaling study and the results obtained from that work. During this effort we reviewed critical issues and design constraints as a function of blade length in the range from 30 meters to 70 meters. The results have been summarized in dimensional and non-dimensional format to aid in interpretation. These results form the baseline for the upcoming assessment of blade cost and have been used to guide our review of potential innovative design approaches.

1.2 Blade Planform Definition

The parametric study reviewed five blade sizes ranging from 30 meters to 70 meters in length. The blade planform characteristics were defined non-dimensionally as a function of the rotor radius, as shown in Table 1.1 and Figure 1.1 and scaled to match each blade length in the study list.

Table 1.1 Non-Dimensional Blade Planform Definition

Radius Ratio	Chord Ratio	Twist (deg)
5%	5.2%	29.5
15%	7.8%	19.5
25%	8.6%	13.0
35%	7.6%	8.8
45%	6.6%	6.2
55%	5.7%	4.4
65%	4.9%	3.1
75%	4.0%	1.9
85%	3.2%	0.8
95%	2.4%	0.0

Figure 1.1 Drawing of Non-Dimensional Blade Planform

The wind turbine was assumed to have a conventional, three bladed rotor with the blades mounted at the root to a central hub. The size of rotor hub was estimated to increase linearly with blade length (Table 1.2).

Table 1.2 Turbine Rotor Characteristics

Blade Length (m)	Hub Radius (m)	Rotor Diameter (m)	Rotor Diameter (ft)
30	1.0	62	203
40	1.5	83	272
50	2.0	104	341
60	2.5	125	410
70	3.0	146	479

1.3 Performance Model

The parametric study used a non-dimensional performance model to estimate turbine performance. The model assumed constant non-dimensional rotor performance, which is provided in Table 1.3. The blades were assumed to operate at constant speed and pitch angle, with peak power output limited only by aerodynamic stall. Modeling the performance of the thicker and thickest airfoils was not within the scope of this work, but additional studies may be performed in later efforts.

The performance model was used to calculate turbine rotational speed and power performance characteristics over a range of blade tip speeds from 60 to 70 m/s, which brackets the operating range of typical commercial wind turbines (Table 1.4).

Drivetrain performance losses were included in the performance model. The basic turbine rating was fixed for each turbine based upon the peak power generated at a tip speed of 70 m/s. The gearbox rating was increased by a 1.5 service factor, while the generator was assumed to have a 1.15 service factor (Table 1.5). The gearbox efficiency was determined from the load factor (rotor power / gearbox rating) assuming the values provided in Table 1.6. The generator efficiency was determined from the load factor (gearbox power / generator rating) assuming the values provided in Table 1.7. A set of example power curves for the 30 meter blade case is presented in Figure 1.2.

Table 1.3 **Non-Dimensional Rotor Performance**

Tip Speed Ratio	Power Coeff. Cp	Thrust Coeff. Ct
18.00	0.128	1.217
15.00	0.311	1.098
13.00	0.403	1.019
12.00	0.443	0.979
11.00	0.479	0.940
10.00	0.506	0.896
9.00	0.516	0.842
8.00	0.505	0.774
7.50	0.489	0.733
7.00	0.472	0.692
6.50	0.449	0.646
6.00	0.429	0.603
5.50	0.387	0.532
5.00	0.288	0.416
4.50	0.207	0.327
4.25	0.175	0.292
4.00	0.147	0.260
3.75	0.123	0.233
3.50	0.102	0.209

Table 1.4 **Turbine Rotational Speeds**

Blade Length (m)	Rotor Speed		
	60 m/s (rpm)	65 m/s (rpm)	70 m/s (rpm)
30	18.5	20.0	21.6
40	13.8	15.0	16.1
50	11.0	11.9	12.9
60	9.2	9.9	10.7
70	7.8	8.5	9.2

Table 1.5 **Turbine Component Power Ratings**

Blade Length (m)	Basic Rating (MW)	Gearbox Rating (MW)	Generator Rating (MW)
30	1.4	2.1	1.6
40	2.5	3.8	2.9
50	4.0	6.0	4.6
60	5.6	8.4	6.4
70	7.6	11.4	8.7

Table 1.6 Non-Dimensional Gearbox Efficiency

Load Factor	Gearbox Efficiency
0.0%	1.0%
2.5%	70.0%
5.0%	80.0%
10.0%	89.0%
20.0%	94.0%
30.0%	96.0%
40.0%	97.0%
50.0%	98.0%
100.0%	98.0%

Table 1.7 Non-Dimensional Generator Efficiency

Load Factor	Generator Efficiency
0.0%	1.0%
10.0%	83.5%
20.0%	90.0%
40.0%	91.5%
60.0%	91.5%
80.0%	91.0%
100.0%	89.5%

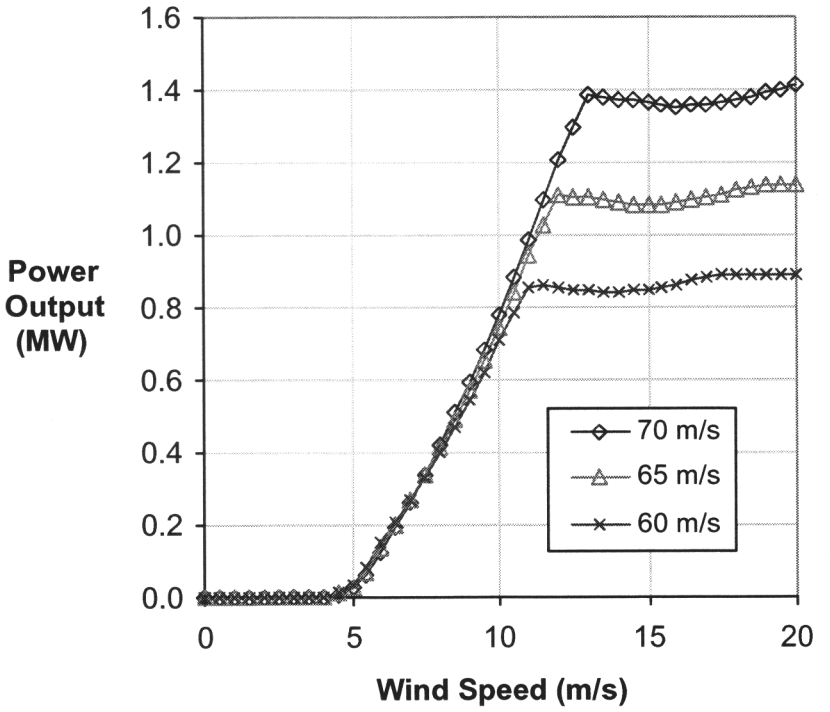

Figure 1.2 30 Meter Blade Power Curves for Various Tip Speeds

1.4 Blade Thickness Definition

Blade section structural properties were estimated for three spanwise thickness distributions (Table 1.8 and Figure 1.3). The baseline, or "thin", distribution represents conventional airfoils used in large wind turbine blades. The "thicker" and "thickest" distributions utilize airfoils that have significantly increased thickness to improve structural performance and reduce weight. All blades evaluated in the study used the same non-dimensional chord and twist distributions.

Table 1.8 Non-Dimensional Blade Thickness Distribution

Radius Ratio	Thickness Ratio (t/c)		
	Baseline	Thicker	Thickest
5%	100%	100%	100%
15%	42%	52%	62%
25%	28%	38%	48%
35%	24%	32%	40%
45%	23%	27%	33%
55%	22%	24%	26%
65%	21%	21%	21%
75%	20%	20%	20%
85%	19%	19%	19%
95%	18%	18%	18%

Aerodynamic data for airfoils with thickness ratios in excess of 30% are not available in the literature. For that reason, the lift and drag characteristics of these airfoils were estimated as part of the parametric study to quantify the effect of increased thickness on airfoil performance characteristics.

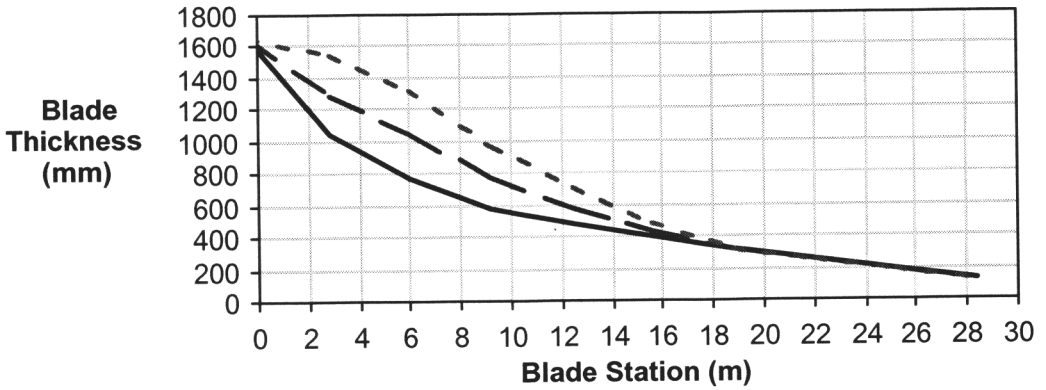

Figure 1.3 30 Meter Blade Thickness as Function of Radial Station for Three Thickness Variations

1.5 Blade Structural Scaling

The blade cross-section structural characteristics were estimated at five spanwise locations (15%, 25%, 45%, 65%, and 85% of radius). The baseline "thin" blade sections were based upon the ERS-100 reference blade [1] and scaled to match the proper chord

length for 30 meter, 50 meter, and 70 meter blade sizes. In addition, blade sections for each of the three blade lengths were evaluated using three blade thickness distributions. Blade sections were scaled linearly (XY scaling) to achieve the specified thickness ratios (see Table 1.8) for each of the three thickness distributions evaluated in the structural analysis (Figures 1.4, 1.5, and 1.6).

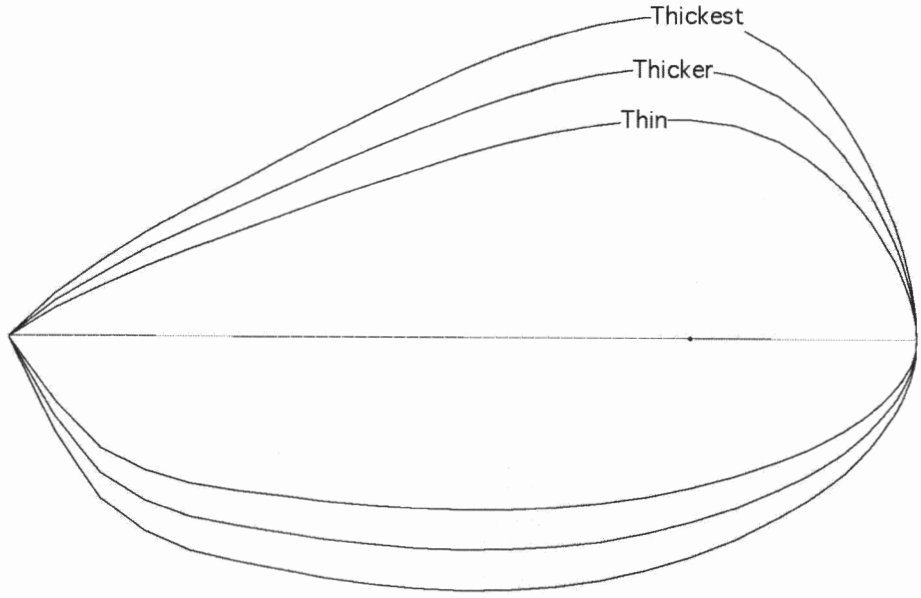

Figure 1.4 Illustration of Blade Sections at 15% Span

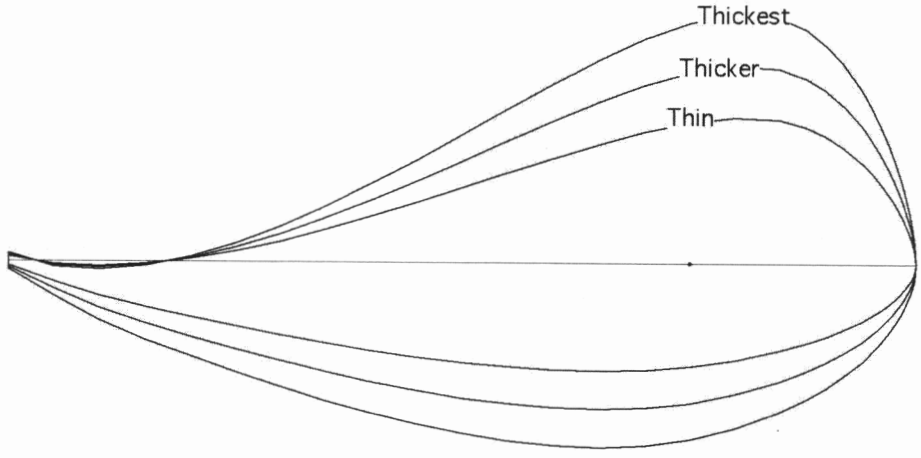

Figure 1.5 Illustration of Blade Sections at 25% Span

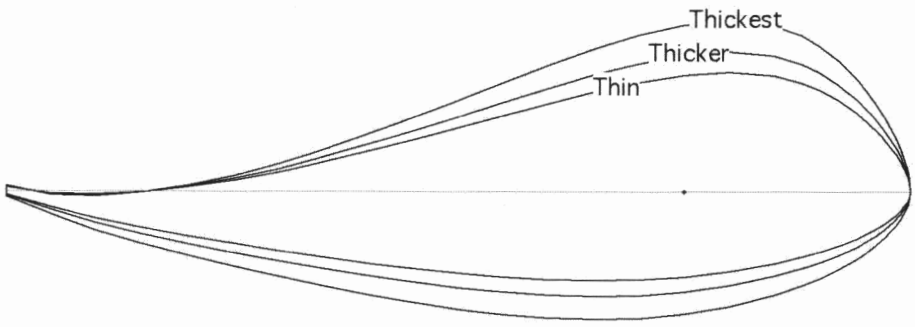

Figure 1.6 Illustration of Blade Sections at 45% Span

1.6 Blade Structural Analysis

Structural analyses of three representative blades (baseline or "thin", "thicker", and "thickest") were performed at representative spanwise stations. The evaluation approach used a beam section analysis methodology that has been successfully applied in previous blade development projects [2,3,4]. The properties of the blade cross-sections were computed using standard two-dimensional beam theory.

The blade construction was assumed to be a stressed shell, which was composed of four primary components: a low pressure (LP) shell on the downwind side, a high pressure (HP) shell on the upwind side, and two shear webs bonded between the two shells as shown in Figure 1.7.

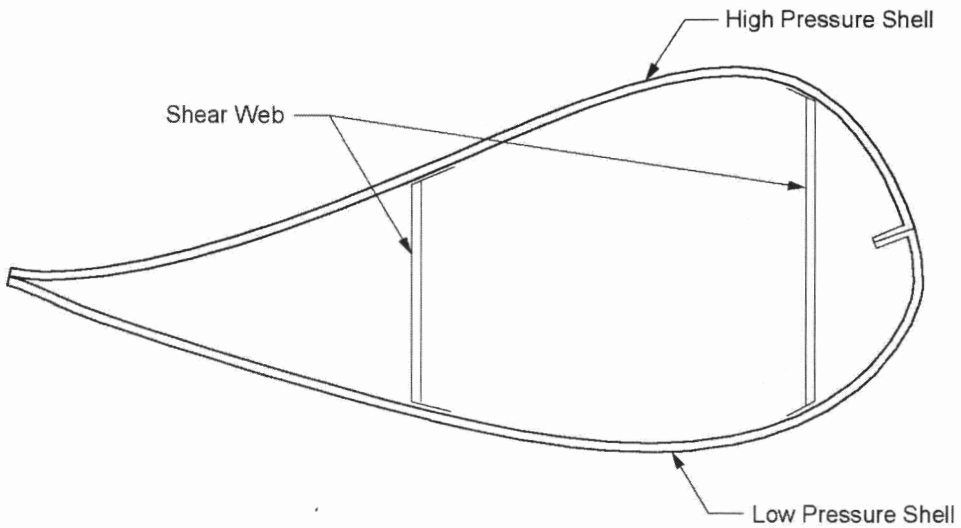

Figure 1.7 Typical Blade Construction

The blade shells were assumed to have e-glass skins. The skins were assumed to fabricated from DBM fabric, which is a double bias (±45°) material backed with continuous strand mat. The e-glass skin layers were separated by balsa coring in the aft panels to provide buckling stability. A structural spar cap composed of uni-directional (0°) e-glass material was assumed to be located in each shell between the shear webs. The two shear webs were assumed to be composed of double bias e-glass fabric with balsa

coring. The DBM fabric that is the primary skin structure was assumed to increase linearly in thickness with blade length. It was taken to be 3.05e-5 of the length. For a 50m blade, this would be 1.5mm (.06"). The outside of the skin was assumed to have .13mm (.005") of gelcoat to provide UV protection, and .38mm (.015") of random mat to suppress print through of the DBM fabric. The gelcoat and random mat thicknesses were held constant.

The shear web core thickness was taken to be 3% of the airfoil thickness. This reflects the fact that the webs of thicker airfoils will have to span a longer top to bottom distance, and will therefore need a thicker core to resist buckling loads. The shear web skins were taken to be 5/3 the thickness of the blade skins, a value which was found sufficient to handle the estimated peak web shear loads. Table 1.9 below summarizes the structural details assumed for this study.

Table 1.9 Summary of Structural Details

Item ID No.	Material Description	Placement Description	Tensile Modulus (Msi)	Layer Width (% of chord)	Layer Thickness (in)	Placement Behind L.E. (% of chord)
1	Gelcoat	Outer Skin	0.50	100%	0.005	0%
2	3/4 oz CSM	Outer Skin	1.10	100%	0.015	0%
3	DBM	Outer Skin	1.39	100%	(A)	0%
4	DBM	Spar Cap Reinf.	1.39	45%	2/3 of (A)	0%
5	C260/520 Uni	Spar Cap (at max)	5.41	30%	(B)	15%
6	DBM	Spar Cap Reinf.	1.39	45%	2/3 of (A)	0%
7	Balsa	Aft Panel	0.02	45%	1%	45%
8	DBM	Inner Skin	1.39	100%	(A)	0%
9	Excess Resin	Inside Inner Skin	0.50	100%	0.030	0%
10	Balsa	35% Web Core	0.02	see note	3% of airfoil	35%
11	DBM	35% Web Skin	1.39	see note	see note	35%
12	C260/520 Uni	T/E spline @ 95%	5.41	6%	(C)	92%
13	TE Plexus	To 2" fwd of TE	0.05	2%	fill gap	98%

Notes

(A) thousandths = 1.2 * blade length 50m -> .060"
(B) this value is found by converging to the required flatwise moment at 3,750 µs
(the spar cap is twice as thick at its center as at its edges)
(C) this value is found by converging to the required edgewise moment at 1,250 µs

For 15% Station
The spar cap width is 60% of chord
The spar cap begins at 5% of chord
The spar cap reinforcement ends at 65% chord
For Shear Web
The balsa thickness was 3% of max airfoil thickness
The height was half the section height (so each half reaches center)
Skins (thousandths) = 2* blade length 50m -> 0.100" each skin

In the table above DBM refers to a fabric which is dominated by +/- 45 degree "double bias" (DB) fibers which has been stabilized by a Continuous Strand Mat (CSM) layer and has been identified in this work as DBM (Double Bias Mat). The balsa placement at 35% refers to the location of the shear web for torsion calculations (i.e. the airfoil volume is broken up into forward and aft cells at 35% of chord).

The bonding adhesive used to join the blade shells, called Plexus, is very low modulus, and so makes an insignificant contribution to flatwise and edgewise bending stiffnesses. It was not modelled at the forward and web joints to simplify the data cases, and was included in the aft joint primarily to capture it mass effect aft in the section.

The design strain value (notes B and C) were defaults selected to give the section property calculations a common basis for comparison. They were selected as typical of values used in design, rather than being tied to specific material and material factor choices.

All of the airfoil shaped stations (outboard of station 25% r/R) have the spar cap beginning at 15% of chord, and extending aft to 45% of chord (See Table 1.9). Station 15% r/R is more of an oval transition shape, and its chord is shortened, so the spar cap would be too narrow and in an inefficient part of the shape, if the values were not adjusted.

Spar cap thickness was derived from the imposed load in an iterative fashion. As the foil thickness increases, the spar cap becomes thinner because the separation between tension and compression side material increases. Table 1.10 shows the spar cap results for each of the blade lengths and thickness distribution variations. The percentage thickness numbers are as a percentage of airfoil thickness.

Table 1.10 Non-Dimensional Blade Thickness Distribution

	Station	Section Thickness		Spar Cap Thickness (ins)			Spar Cap / Section Thickness (%)		
	(%)	(mm)	(ins)	baseline	thicker	thickest	baseline	thicker	thickest
30 meter	85	188	7.40	0.361			4.9%		
	65	317	12.48	1.011			8.1%		
	45	473	18.62	1.548	1.234	0.944	8.3%	6.6%	5.1%
	25	746	29.37	1.548	1.045	0.779	5.3%	3.6%	2.7%
	15	1009	39.72	0.870	0.66	0.521	2.2%	1.7%	1.3%
50 meter	85	315	12.40	0.650			5.2%		
	65	532	20.94	1.755			8.4%		
	45	794	31.26	2.639	2.103	1.621	8.4%	6.7%	5.2%
	25	1252	49.29	2.631	1.778	1.327	5.3%	3.6%	2.7%
	15	1693	66.65	1.477	1.124	0.9	2.2%	1.7%	1.4%
70 meter	85	443	17.44	0.922			5.3%		
	65	747	29.41	2.493			8.5%		
	45	1114	43.86	3.706	2.947	2.256	8.4%	6.7%	5.1%
	25	1758	69.21	3.693	2.489	1.851	5.3%	3.6%	2.7%
	15	2376	93.54	2.039	1.526	1.202	2.2%	1.6%	1.3%

1.7 Blade Design Loads

Blade design loads were estimated using two simplified methods: parked under extreme winds and an operating gust condition. The first model calculated the extreme loads with the turbine in the parked condition in accordance with IEC and Germanisher Lloyd Class I design recommendations (Table 1.11). This method assumed the wind speed was 70 m/s at the rotor hub and wind shear increased with hub height according to $1/7^{th}$ power law with an exponent of 0.143. Sea level air density was assumed and a partial load factor of 1.35 was included in the analysis. Blade extreme design loads are based on flat plate

drag coefficients and the different thickness distributions (baseline "thin", "thicker", and "thickest") were evaluated using the same loads.

The second calculation method estimated blade spanwise loading under high wind gust conditions. A blade element momentum model calculated loads at 10 radial locations, which were integrated to determine the bending moment on the blade. Under this loading scenario the turbine was considered to be operating at constant speed during a 55 m/s gust. Both load estimation approaches provided similar results as shown in Figure 1.8.

Table 1.11 30 m Blade Extreme Moment Loading Results

Rotor Radius	31.0	m	
Hub Height	60	m	
Blade Azimuth	0	deg	Blade Tip Upward
Design Wind Class	1		
Hub Height Wind Speed	70.0	m/s	
Air Density	1.225	kg/m^3	
Wind Shear	0.14		
Load Factor	1.35		

Rotor Station (%)	Twist Angle (deg)	Chord Length (m)	Wind Speed (m/s)	Drag Coeff. Cd	Thrust Force (kN)	Bending Moment (kNm)
0%	29.5	1.603	70.0	0.80	308	4240
10%	19.5	2.403	70.5	1.45	294	3307
20%	13.0	2.666	71.0	1.45	252	2460
30%	8.8	2.348	71.5	1.45	204	1754
40%	6.2	2.058	71.9	1.45	160	1191
50%	4.4	1.780	72.3	1.45	120	757
60%	3.1	1.510	72.8	1.45	86	438
70%	1.9	1.247	73.2	1.45	56	219
80%	0.8	0.989	73.6	1.45	31	83
90%	0.0	0.735	73.9	1.10	11	18

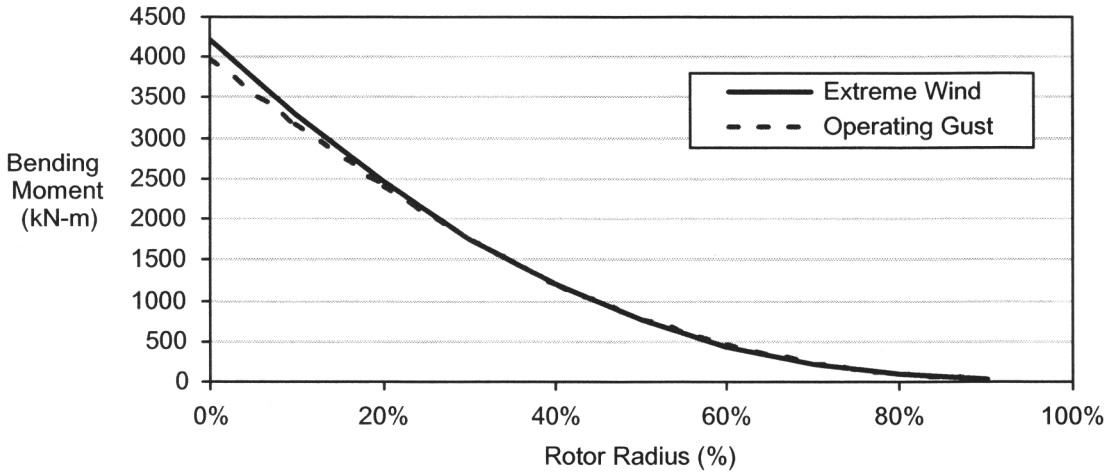

Figure 1.8 Comparison of 30m Blade Loads for Two Analysis Approaches

1.8 Blade Aerodynamic Scaling

The aerodynamic properties of the thick airfoils assumed in the structural analysis were not available from the literature. Typically, the maximum airfoil thickness to chord ratio is limited to approximately 24%; e.g., Abbott & Von Doenhoff [5] do not report any results for airfoils thicker than 24%. Also, the NREL laminar flow airfoil series for horizontal-axis wind turbines stops at maximum thickness-to-chord ratios of 26%. As stated by Tangler & Somers [6], maximum thickness ratios greater than 26% were deemed to have unacceptable aerodynamic performance characteristics.

However, structural analyses for very large blades indicate that thicker airfoils are necessary to limit the growth in blade structural weight and, hence, blade cost with increasing turbine size. As a result it was necessary to estimate the aerodynamic characteristics of the thick airfoil sections. An aerodynamic scaling effort was undertaken in parallel with the structural analysis work to evaluate the effect of extreme thickness on aerodynamic characteristics.

Two programs developed by Morgan at NASA Langley were used to smooth and scale the airfoil coordinates [6]. The smoothing program utilizes least-squares polynomials and least-squares cubic spline techniques to smooth the second derivatives of the z-axis airfoil coordinates with respect to a transformed x-axis coordinate. The resulting smooth airfoil coordinates are then determined by solving a tri-diagonal matrix of simultaneous cubic spline equations relating the z-axis coordinates and their corresponding second derivatives. A technique for splitting the airfoil z-axis coordinates in its camber distribution and its thickness distribution is used to define the airfoil shape. Next, the scaling program uses this information to modify the thickness distribution to a specified thickness, which is then combined with the original camber distribution to obtain the scaled-airfoil geometry. The advantage of this methodology is that the scaling process does not modify the camber distribution, which governs the zero-lift angle of attack, and the design lift coefficient.

The NREL S821 was selected as the baseline airfoil used in the aerodynamic scaling study. A series of scaled airfoil versions were developed and analyzed. The maximum thickness-to-chord ratio was modified in increments of approximately 5%, starting at 24% for the S821 and ending with an extreme design case of 60% t/c. The resulting airfoil family is shown in Figure 1.9.

It is important to note that the structural analysis assumed simple XY scaling based upon an earlier blade design (Reference 1). This method resulted in section shapes that differed from those developed with an aerodynamically consistent scaling approach (Figure 1.10). While aerodynamic scaling retains the mean line and camber of the original airfoil during scaling, the simple XY scaling distorted those characteristics. Although the XY scaling used in the structural work was different than the aerodynamic scaling used here, it did not present a problem for this work because we were interested in evaluating the general trends under varying blade thickness and both of the methods were applied consistently for each thickness within the separate analyses.

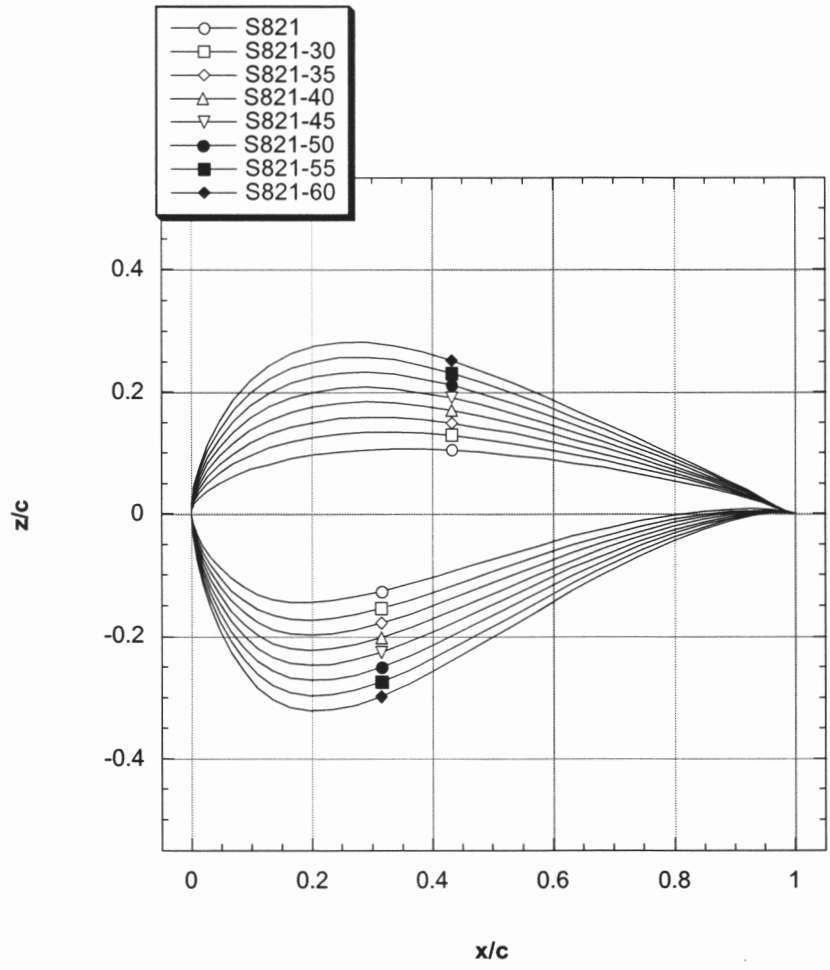

Figure 1.9 Aerodynamically Scaled Airfoil Thickness Distribution

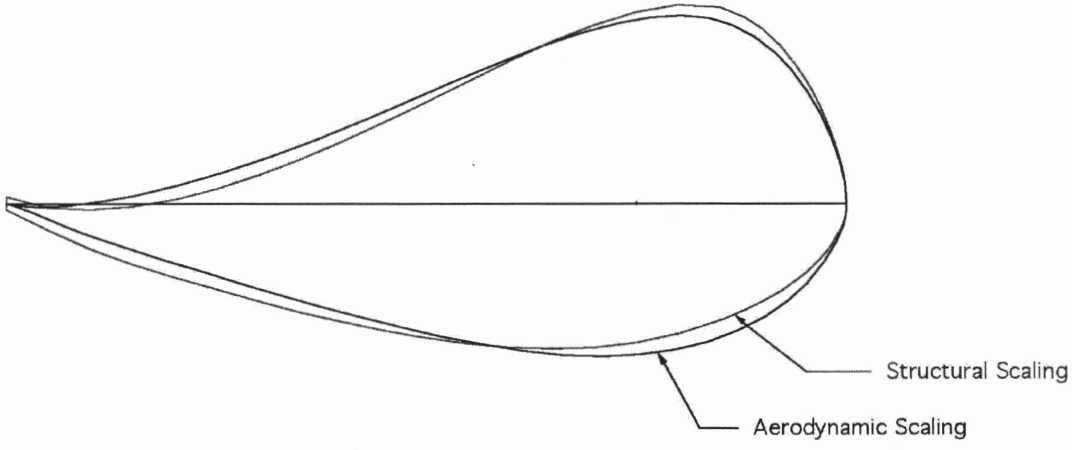

Figure 1.10 Comparison of Airfoil Shapes Developed Using Structural and Aerodynamic Scaling Methods

1.9 Thick Airfoil Properties

The properties of the aerodynamically scaled thick airfoils were determined using the airfoil analysis method MSES by Drela [7]. This viscous/inviscid interaction method is a direct extension of the single-element viscous/inviscid methodology employed in the ISES code [8,9]. The model is capable of predicting transitional bubbles, shock waves, and flow separation. Boundary-layer transition can be fixed (user defined trip location) or predicted using a semi-empirical relationship. Different far-field boundary conditions can be specified including unbounded flow and bounded flow involving solid wall or free-jet conditions.

Drela and others have extensively validated MSES (Reference 7) and have shown that the results generated with this airfoil analysis program agree well with experimental data. Prior success with MSES led to its application for analysis of the aerodynamic characteristics of various blade sections in the present study. An example streamline grid surrounding an NREL S821 airfoil is depicted in Figure 1.11. In this solution the boundary-layer transition location was left free, which represents a natural flow transition. The displacement body representation used to model the shear layers clearly depicts the separation in the trailing-edge region.

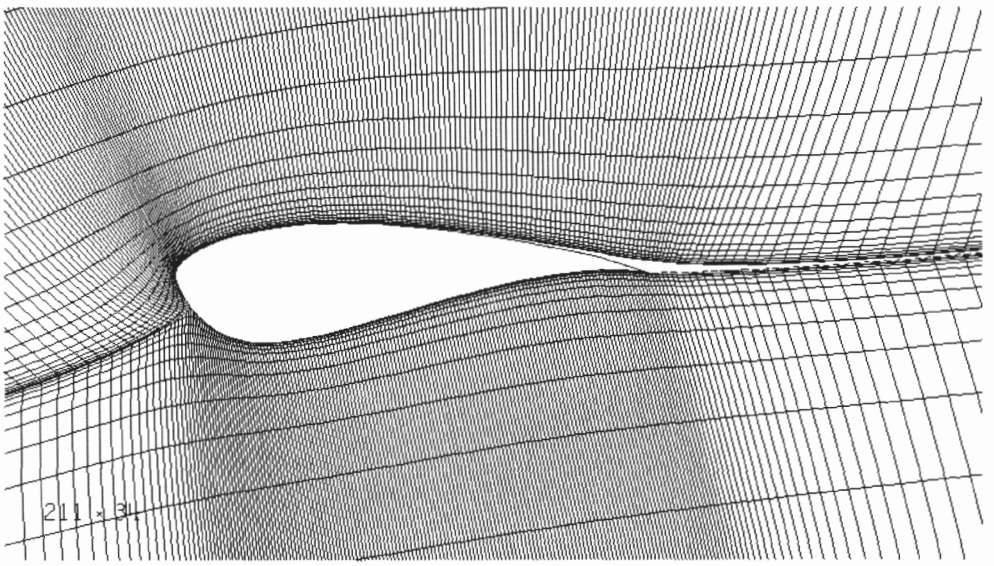

Figure 1.11 Closeup of Streamline Grid About S821 Airfoil for Converged Solution at α = 10.0°, Re = 2.30 million, M_8 = 0.1, Free Transition

2.0 STUDY RESULTS

2.1 Performance Scaling Results

2.1.1 Rotor Performance Scaling

The parametric review estimated maximum rotor power and annual energy capture for megawatt scale wind turbines with rotors of 62, 83, 104, 125, and 146 meters in diameter. The annual energy production for each rotor size was evaluated as a function of tip speed at 60, 65, and 70 m/s. The analysis assumed a Rayleigh wind distribution and did not include losses due to availability, arrays, air density variation, blade soiling, control systems, or electrical distribution. The rotor was assumed to operate at constant speed and with a fixed pitch angle.

As expected, the results show a strong relationship between rotor tip speed and peak power output (Figure 2.1, Tables 2.1 and 2.2). For this study power output was limited by the natural stall characteristics of the rotor. Energy production increased approximately as the square of the rotor diameter. For a given rotor diameter the turbine peak power scaled roughly as the cube of the tip speed. Compared with the 5.5 m/s case, specific energy production increased by approximately 25% and 50% for wind speeds of 6.0 and 6.5 m/s respectively. Specific energy at 70 m/s increased by 11%, 15%, and 18% for each mean wind speed compared to the 60 m/s case.

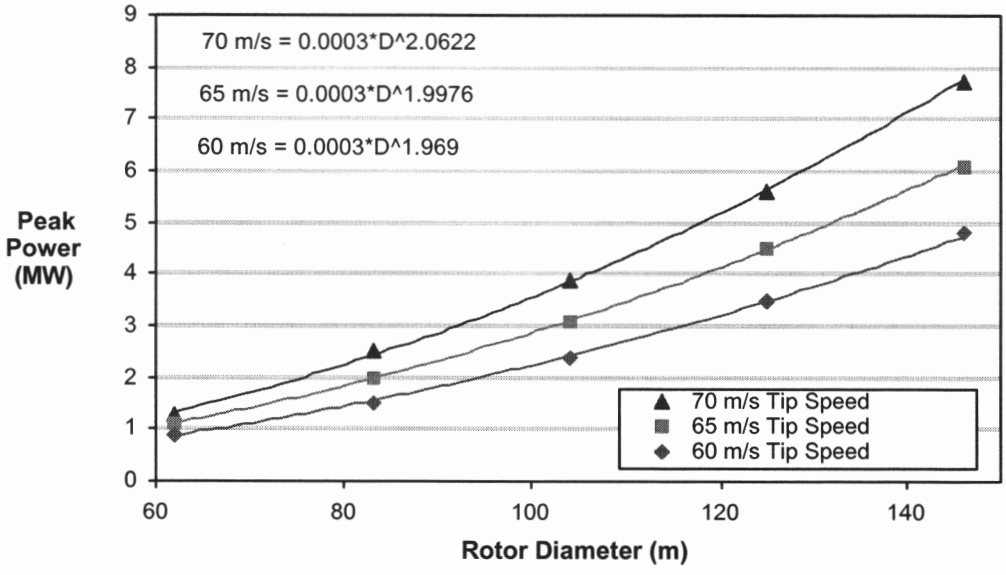

Figure 2.1 Peak Power as a Function of Rotor Diameter and Tip Speed

Table 2.1 Performance as a Function of Rotor Diameter and Tip Speed

Tip Speed	Rotor Diameter (m)	Blade Length (m)	Peak Power (MW)	Annual Energy Production (MWh)		
				5.5	6.0	6.5
60	62	30	0.9	1648	2034	2412
60	83	40	1.5	2965	3646	4324
60	104	50	2.4	4626	5709	6773
60	125	60	3.5	6716	8285	9824
60	146	70	4.8	9170	11311	13411
65	62	30	1.1	1757	2209	2663
65	83	40	2.0	3151	3960	4775
65	104	50	3.1	4932	6202	7480
65	125	60	4.5	7159	8994	10842
65	146	70	6.1	9772	12276	14797
70	62	30	1.3	1824	2330	2853
70	83	40	2.5	3269	4177	5114
70	104	50	3.9	5122	6548	8018
70	125	60	5.6	7425	9482	11603
70	146	70	7.7	10132	12937	15827

Table 2.2 Specific Production as a Function of Rotor Diameter and Tip Speed

Tip Speed	Rotor Diameter (m)	Blade Length (m)	Peak Power (W/m2)	Specific Energy Production (MWh/m2)		
				5.5	6.0	6.5
60	62	30	298	0.55	0.67	0.80
60	83	40	277	0.55	0.67	0.80
60	104	50	283	0.54	0.67	0.80
60	125	60	285	0.55	0.68	0.80
60	146	70	287	0.55	0.68	0.80
65	62	30	364	0.58	0.73	0.88
65	83	40	370	0.58	0.73	0.88
65	104	50	365	0.58	0.73	0.88
65	125	60	367	0.58	0.73	0.88
65	146	70	364	0.58	0.73	0.88
70	62	30	431	0.60	0.77	0.94
70	83	40	462	0.60	0.77	0.95
70	104	50	459	0.60	0.77	0.94
70	125	60	456	0.61	0.77	0.95
70	146	70	460	0.61	0.77	0.95

The performance data were also plotted as contour plots to provide an alternative view of the results. Contours of constant energy capture as a function of rotor diameter and tip speed are provided in Figures 2.2 through 2.4. Again the basic trending shows that annual energy production increases with tip speed, but less strongly than peak power. The maximum benefit available from increased tip speed is obtained at higher wind sites, which have more operational hours at peak power. Increases in peak power will also require larger and more costly drive components, so these plots do not describe the trends in cost of energy.

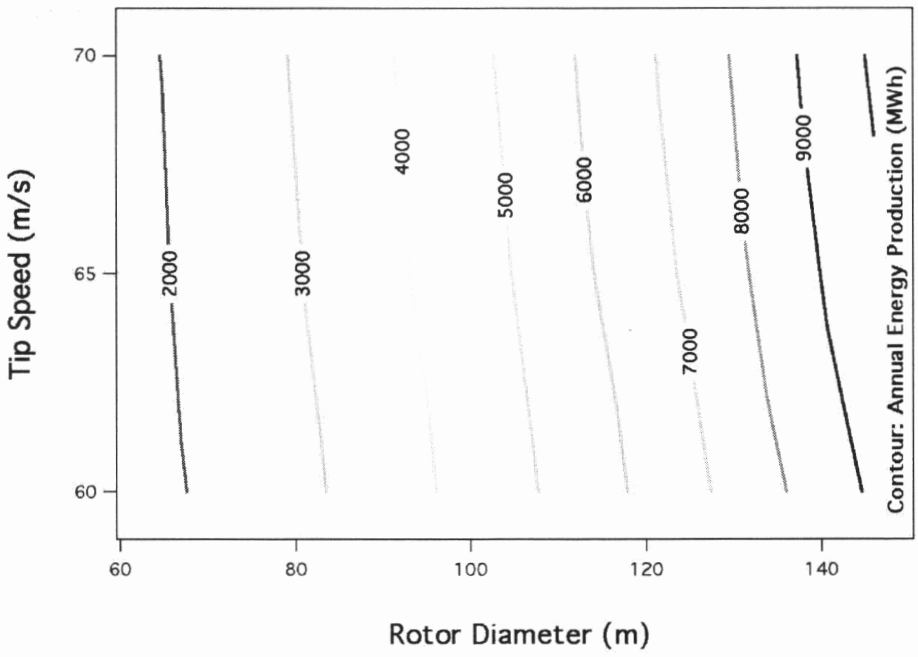

Figure 2.2 **Contour Plot of Energy Production as a Function of Diameter and Tip Speed for a 5.5 m/s Mean Rayleigh Wind Distribution**

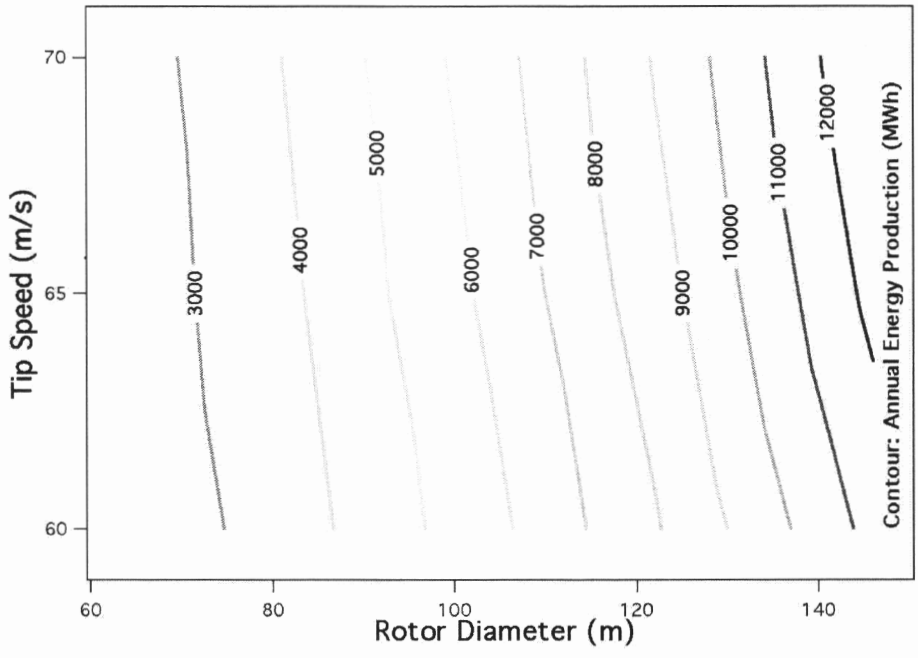

Figure 2.3 **Contour Plot of Energy Production as a Function of Diameter and Tip Speed for a 6.0 m/s Mean Rayleigh Wind Distribution**

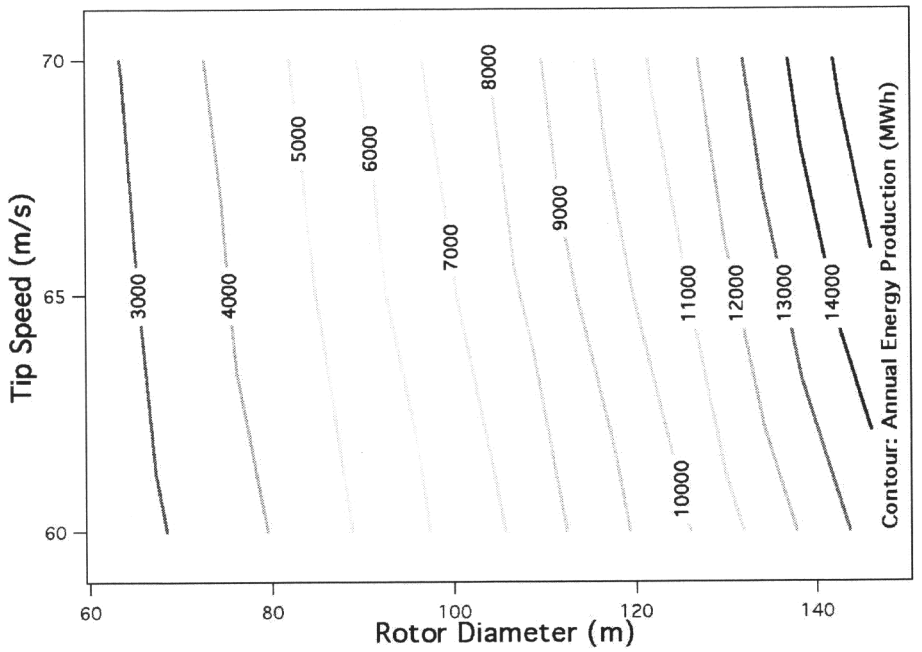

Figure 2.4 Contour Plot of Energy Production as a Function of Diameter and Tip Speed for a 6.5 m/s Mean Rayleigh Wind Distribution

2.2 Structural Scaling Results

2.2.1 Blade Laminate Weight Scaling

The parametric study evaluated the growth in blade laminate weight with rotor scale for each of the three thickness distributions. The analysis included the weight of the blade skins, structural spars, shear webs, and bonding materials. The weight estimate did not include the weight of the root laminate or the metal root fittings, which are specific to a given attachment method. The weight scaling trends as the blade volume and follows a cube law relationship (Figures 2.5 and 2.6 and Table 2.3). The specific weight scales linearly (cube/square) so larger rotors require increasingly more material per unit of swept area (Figures 2.7 and 2.8).

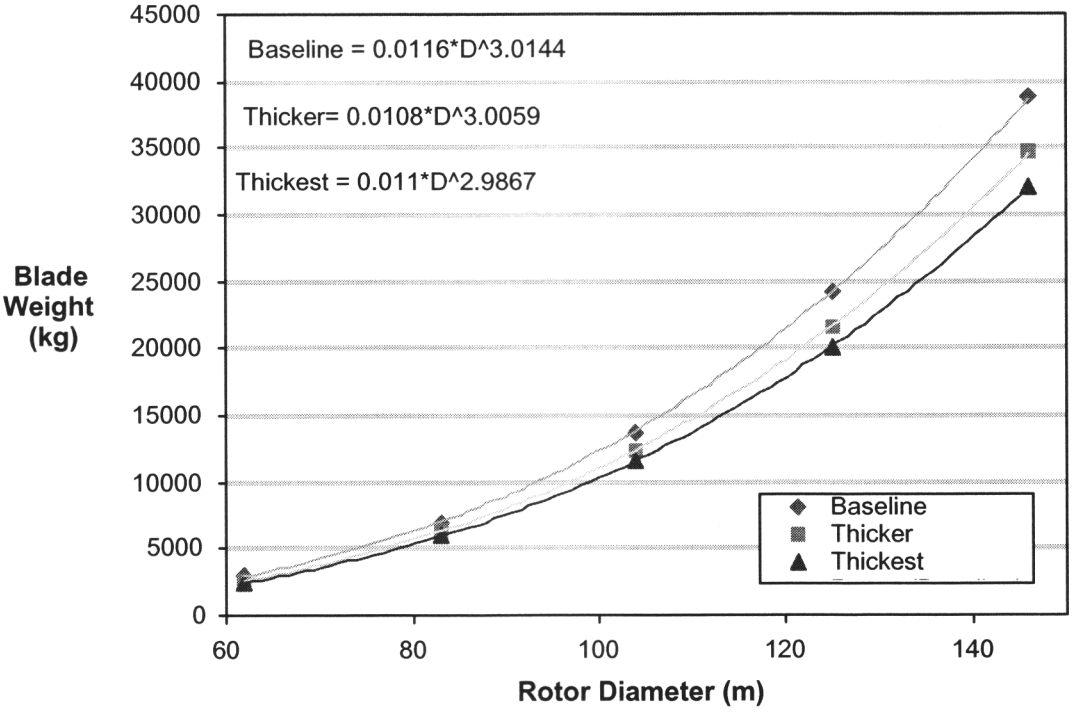

Figure 2.5 Blade Laminate Weight as a Function of Rotor Diameter

Table 2.3 Blade Laminate Weight as a Function of Rotor Diameter

Section Type	Rotor Diameter (m)	Blade Length (m)	Blade Length (ft)	Blade Weight (kg)	Blade Weight (lbm)	Specific Weight (kg/m2)
Baseline	62	30	98	2936	6459	0.97
Baseline	83	40	131	7028	15462	1.30
Baseline	104	50	164	13764	30281	1.62
Baseline	125	60	197	24177	53190	1.97
Baseline	146	70	230	38883	85543	2.32
Thicker	62	30	98	2638	5803	0.87
Thicker	83	40	131	6305	13870	1.17
Thicker	104	50	164	12308	27077	1.45
Thicker	125	60	197	21612	47547	1.76
Thicker	146	70	230	34677	76289	2.07
Thickest	62	30	98	2482	5461	0.82
Thickest	83	40	131	5910	13003	1.09
Thickest	104	50	164	11554	25418	1.36
Thickest	125	60	197	20102	44225	1.64
Thickest	146	70	230	32066	70545	1.92
Thin	62	30	98	2936	6459	0.97
Thicker	104	50	164	12308	27077	1.45
Thickest	146	70	230	32066	70545	1.92

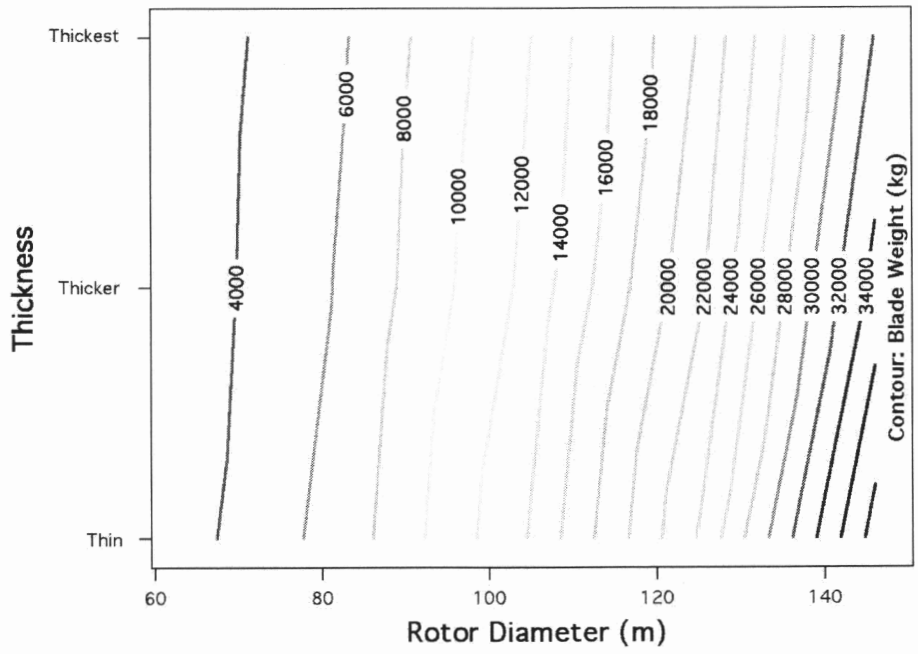

Figure 2.6 Contour Plot of Blade Laminate Weight as a Function of Section Thickness and Rotor Diameter

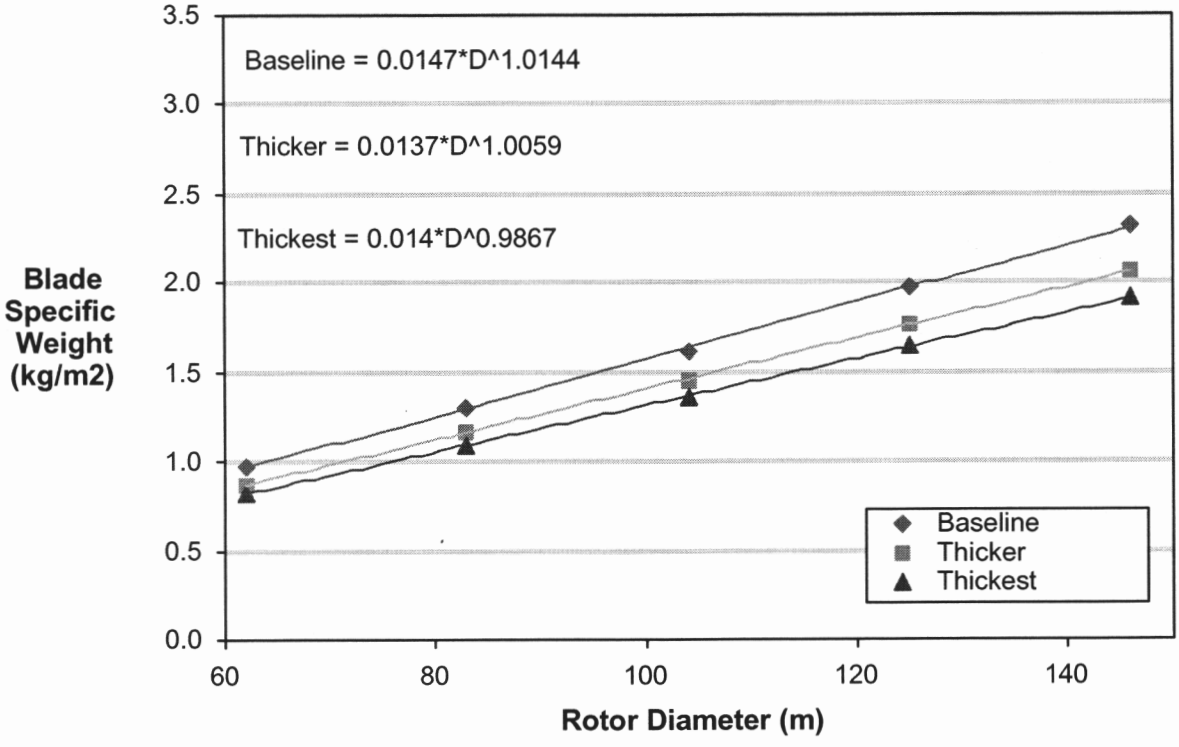

Figure 2.7 Blade Specific Weight as a Function of Rotor Diameter

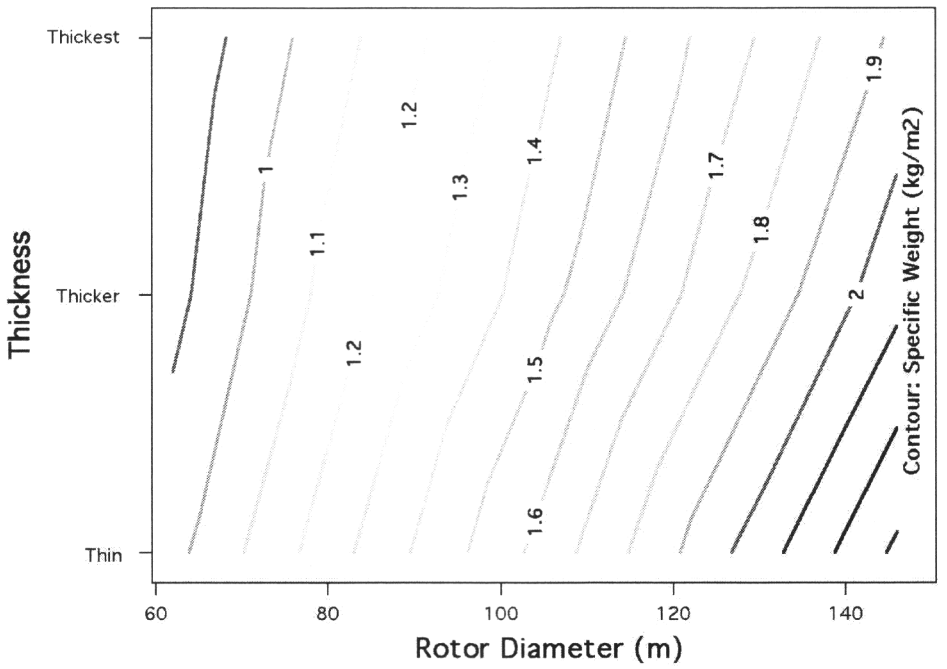

Figure 2.8 Contour Plot of Blade Specific Weight

2.2.2 Tip Deflection Scaling

Blade tip deflection is another major design factor for large wind turbine blades. Tip deflection was calculated assuming an IEC Class I extreme wind (70 m/s) design load case for three blade sizes (30, 50, and 70 meters) and three thickness distributions (thin, thicker, thickest) as shown in Table 2.4 and Figures 2.9 and 2.10. Tip deflection increased approximately as a linear power of diameter. Specific deflection, defined as the tip deflection divided by the rotor diameter, increased in the first half of the analysis range (60 to 100 meters, Figures 2.11 and 2.12), but was roughly constant in the upper band of the range (100 to 150 meters). Again the influence of airfoil section thickness was an important factor on the results.

2.2.3 Simplified Economic Scaling

A simplified economic model was used to show basic trends in the cost of the blades. The energy sales price was assumed to be $5 per MWh. The total cost of the blade was estimated to be $11 per kg and each rotor was assumed to have three blades. Rotor cost was repaid by energy sales and used to calculate simple payback in years. The trends show that payback time more than doubles over the analysis range (Table 2.5 and Figures 2.13, 2.14, and 2.15). This negative economic trend is caused by increased blade weight.

Table 2.4 Blade Tip Deflection as a Function of Rotor Diameter

Section Type	Rotor Diameter (m)	Blade Length (m)	Tip Deflection (m)	Tip Deflection (in)	Specific Deflection (% Diameter)
Baseline	62	30	5.9	233	9.53%
Baseline	83	40	8.2	321	9.83%
Baseline	104	50	10.6	418	10.20%
Baseline	125	60	12.7	501	10.17%
Baseline	146	70	14.9	586	10.20%
Thicker	62	30	5.2	204	8.36%
Thicker	83	40	7.2	282	8.62%
Thicker	104	50	9.3	366	8.93%
Thicker	125	60	11.2	439	8.92%
Thicker	146	70	13.1	514	8.95%
Thickest	62	30	4.6	182	7.44%
Thickest	83	40	6.4	251	7.67%
Thickest	104	50	8.3	325	7.94%
Thickest	125	60	9.9	391	7.94%
Thickest	146	70	11.7	459	7.98%
Thin	62	30	5.9	233	9.53%
Thicker	104	50	9.3	366	8.93%
Thickest	146	70	11.7	459	7.98%

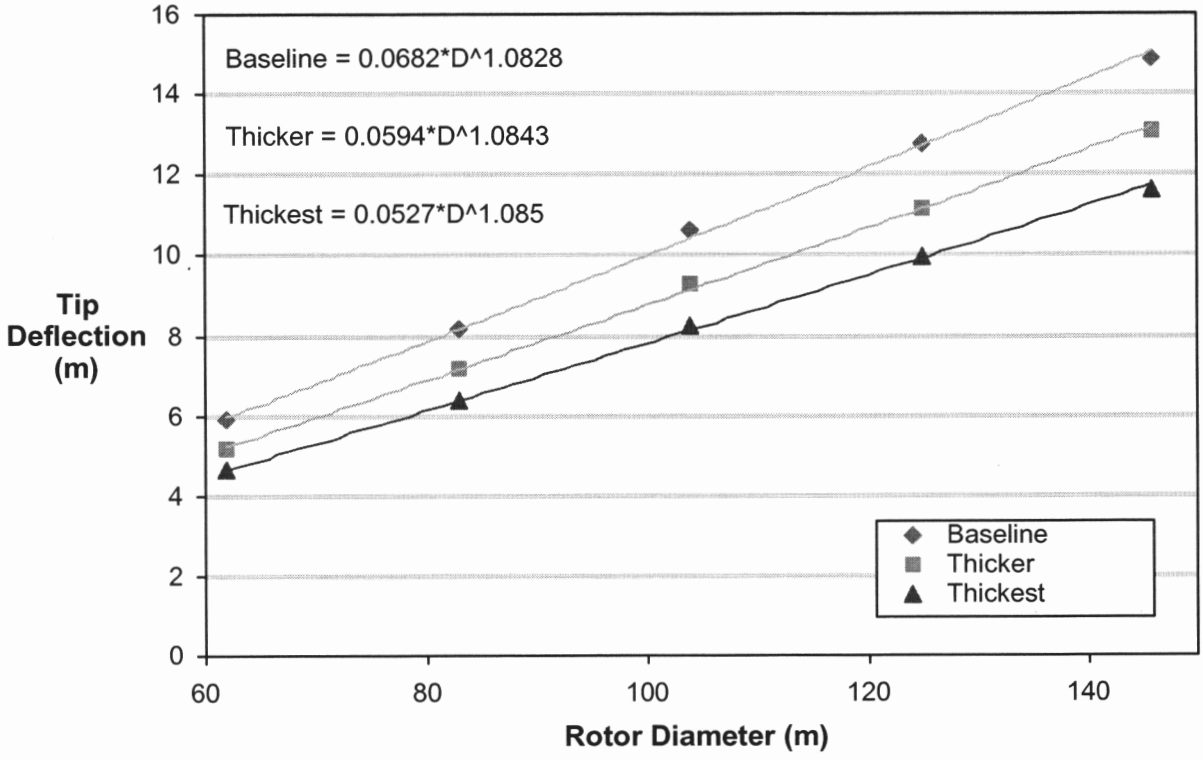

Figure 2.9 Blade Tip Deflection as a Function of Rotor Diameter

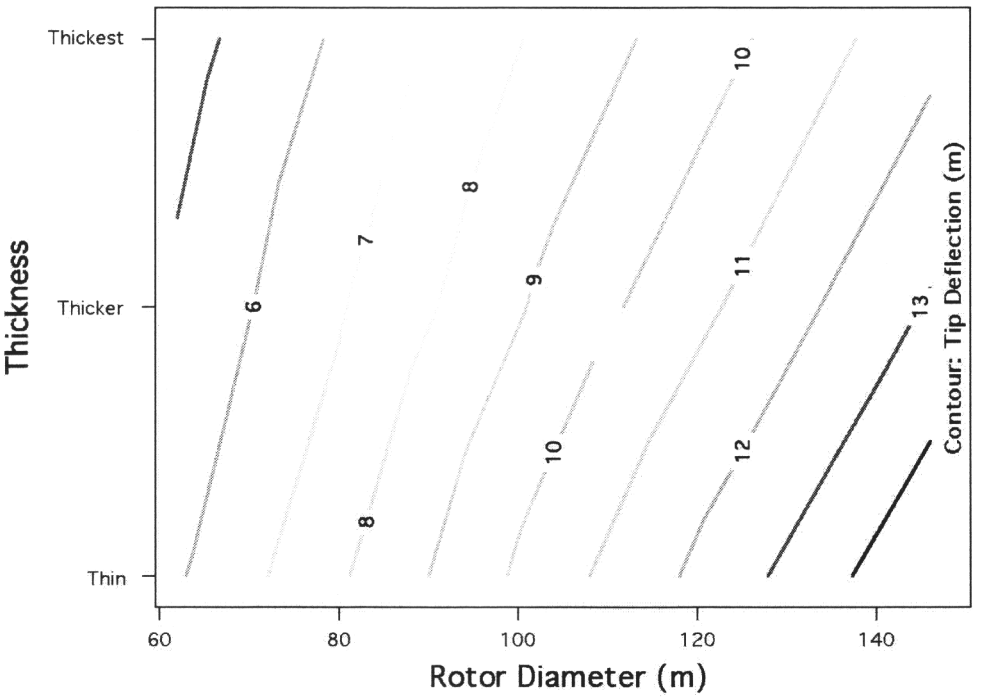

Figure 2.10 Contour Plot of Tip Deflection as a Function of Rotor Diameter

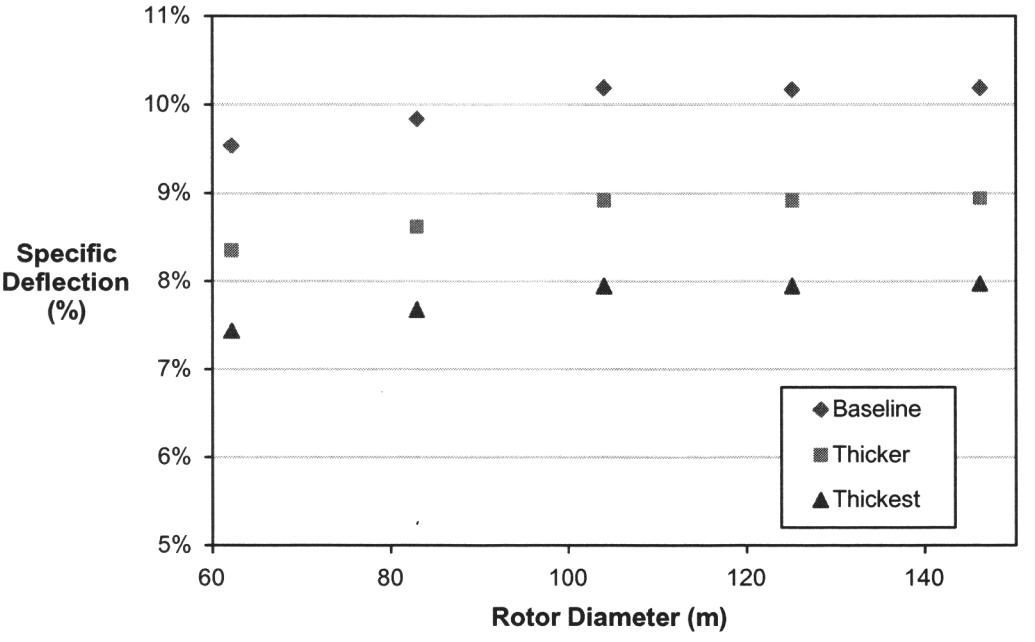

Figure 2.11 Specific Tip Deflection as a Function of Rotor Diameter

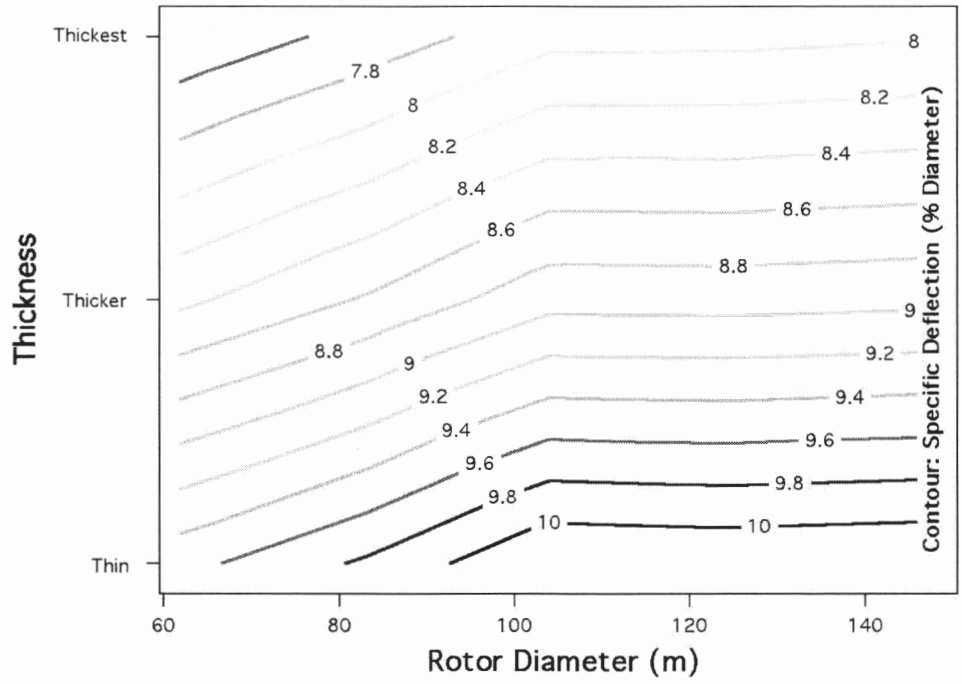

Figure 2.12 Contour Plot of Specific Deflection

Table 2.5 Simplified Economic Scaling Parameters

Section Type	Rotor Diameter (m)	Blade Length (m)	Blade Length (ft)	Rotor Cost ($)	Energy Sales ($)	Rotor Payback (years)
Baseline	62	30	98	96889	101700	0.95
Baseline	83	40	131	231928	182300	1.27
Baseline	104	50	164	454212	285450	1.59
Baseline	125	60	197	797848	414250	1.93
Baseline	146	70	230	1283143	565550	2.27
Thicker	62	30	98	87045	110450	0.79
Thicker	83	40	131	208055	198000	1.05
Thicker	104	50	164	406148	310100	1.31
Thicker	125	60	197	713206	449700	1.59
Thicker	146	70	230	1144334	613800	1.86
Thickest	62	30	98	81916	116500	0.70
Thickest	83	40	131	195046	208850	0.93
Thickest	104	50	164	381274	327400	1.16
Thickest	125	60	197	663370	474100	1.40
Thickest	146	70	230	1058178	646850	1.64

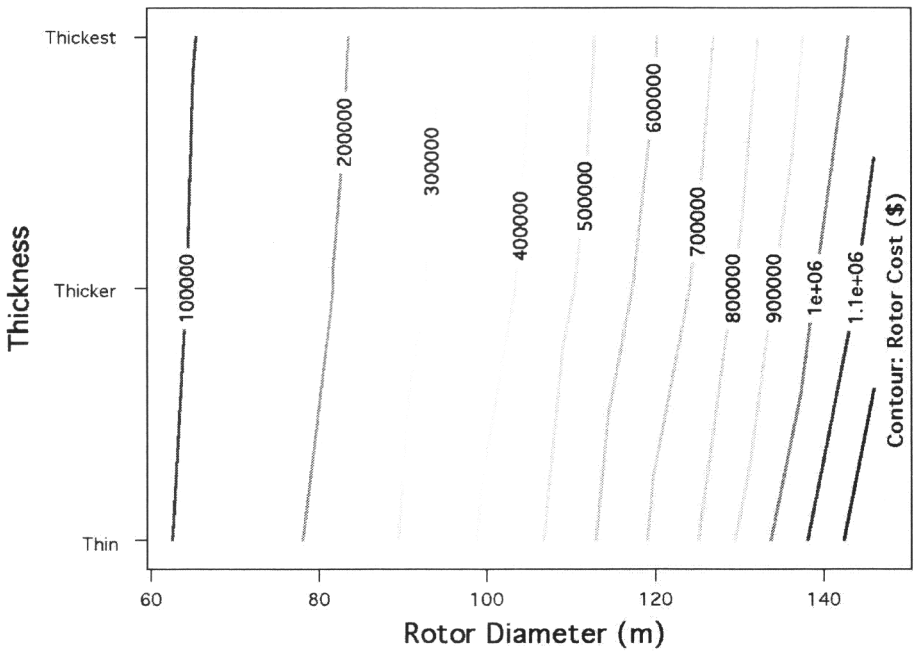

Figure 2.13 Contour Plot of Rotor Cost Scaling

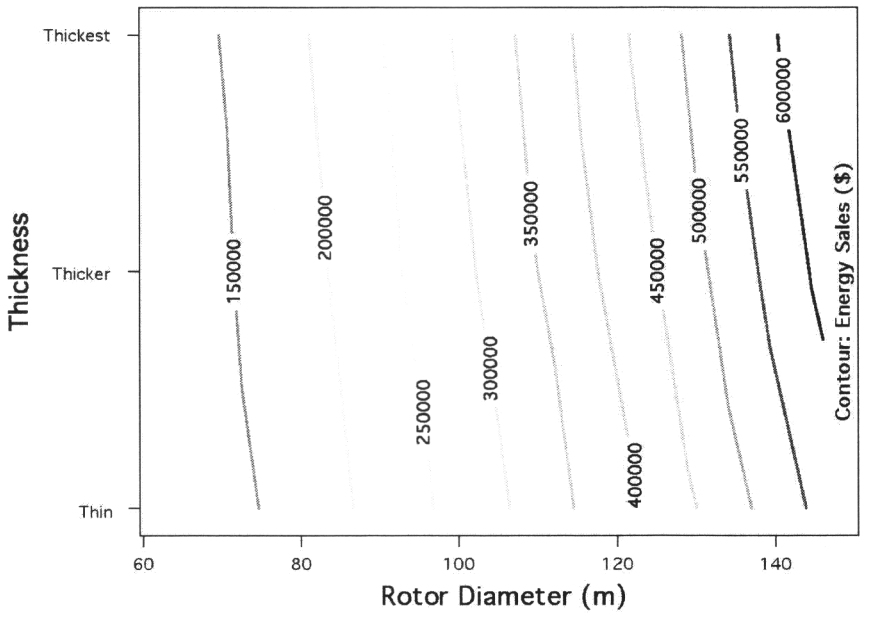

Figure 2.14 Contour Plot of Energy Sales Scaling

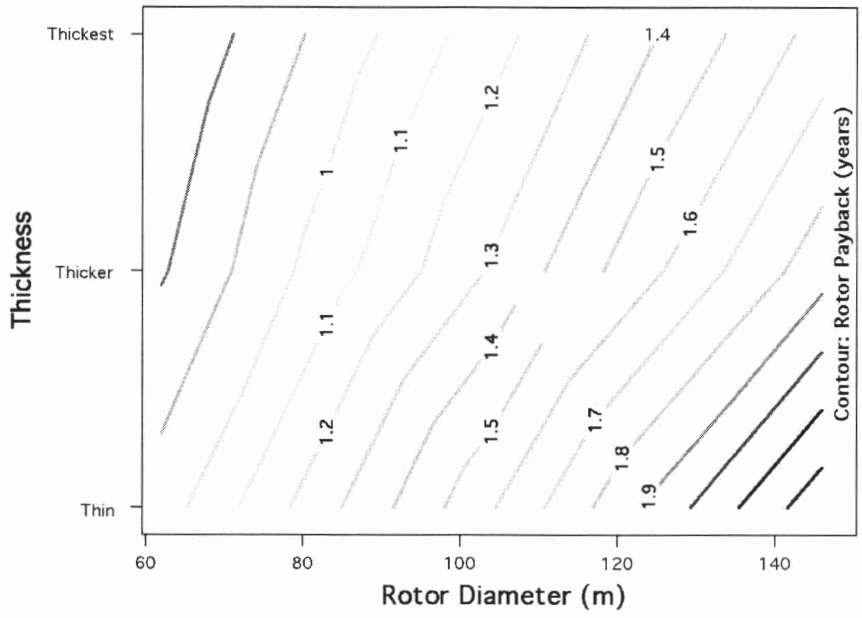

Figure 2.15 Contour Plot of Simple Rotor Payback Scaling

2.3 Airfoil Scaling Results

2.3.1 Effect of Thickness on Aerodynamic Performance

The baseline airfoil utilized in the thickness scaling study is the S821 [5] which has a maximum thickness to chord ratio of 24%. The scope of this work was to provide a preliminary evaluation of the effect of thickness on airfoil performance. This blade-root airfoil was designed to have a high maximum lift coefficient which is largely insensitive to surface-roughness induced premature transition. In Figure 2.16, the lift characteristics of the S821 airfoil calculated using MSES (Reference 7) are shown at a chord Reynolds number of 2.30 million and 4.35 million. These Reynolds numbers are representative of those encountered in the inboard region of large rotors. In all cases the Mach number is kept constant at 0.1. Mach number effects are not considered significant at these conditions. Future studies will focus on compressibility effects in more detail.

The effect of contaminated surfaces was investigated by analyzing the airfoil assuming natural transition as well as fixed transition at x/c = 0.02 on the upper (suction) surface and x/c = 0.05 on the lower (pressure) surface. As expected, lift is largely unaffected by changes in the transition location. The most important performance numbers for the S821 are summarized in Table 2.6. Note that the calculations were typically terminated at α = 16°. The lift curves show that maximum lift is reached near this angle but slightly higher lift coefficients may be achievable for angles in excess of 16°.

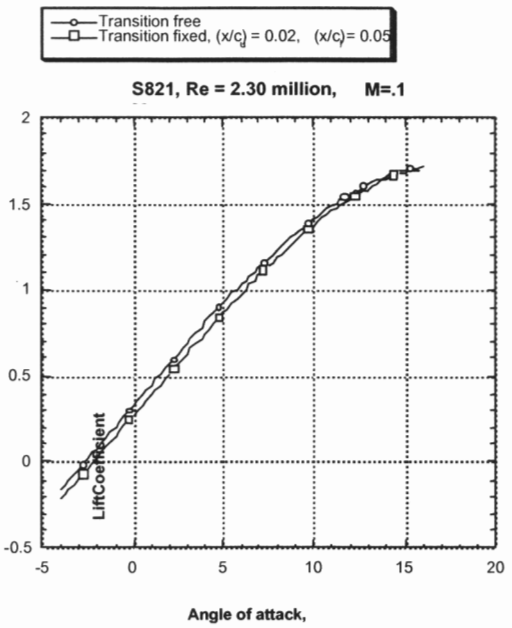

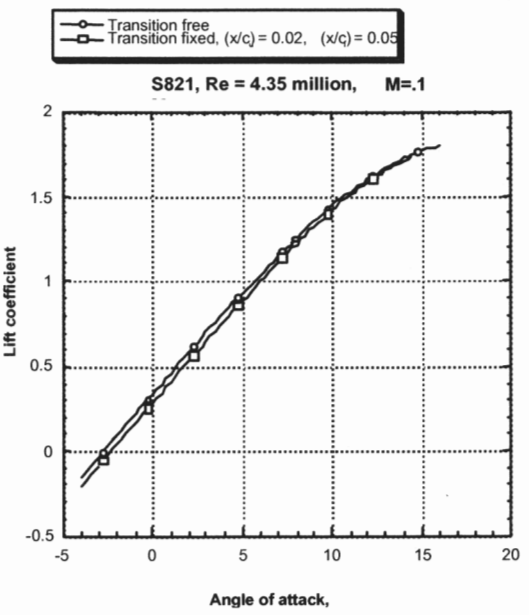

Figure 2.16 Lift Characteristics of S821 Airfoil at Re = 2.30 million and Re = 4.35 million, Free and Fixed Transition

Table 2.6 Aerodynamic Performance Characteristics of the S821 Airfoil

	RE = 2.30 MILLION		RE = 4.35 MILLION	
	FREE	FIXED	FREE	FIXED
α_{0} /(DEG)	-2.643	-2.191	-2.743	-2.322
C_{L_O}	0.324	0.266	0.337	0.284
C_D @ C_{L_O}	0.0080	0.0127	0.0072	0.0114
$(C_L/C_D)_{MAX}$	100.1	78.7	103.5	92.3
C_L @ $(C_L/C_D)_{MAX}$	0.951	1.349	0.877	1.463
$C_{L_{MAX}}$	1.716	1.692	1.803	1.730
α_{max} /(DEG)	16.0	15.875	16.0	14.5

The effect of thickness on airfoil lift is depicted in Figures 2.17 and 2.18 for free and fixed transition, and Re = 2.30 million and 4.35 million, respectively. At the lower Reynolds number converged steady flow solutions were only achievable for airfoils with t/c ≤ 0.40-0.45. At the higher Reynolds number converged steady solutions were obtained for the entire family given transition free conditions and for airfoils with t/c ≤ 0.45 with transition fixed near the leading edge.

The results show that at transition free conditions airfoil maximum lift coefficient peaks at t/c = 0.35. However, with transition fixed near the leading edge all airfoils except the baseline airfoil encounter a drop in maximum lift coefficient. Note that redesigning the thickened airfoils and/or the addition of vortex generators on the suction surface may reduce this sensitivity to premature transition.

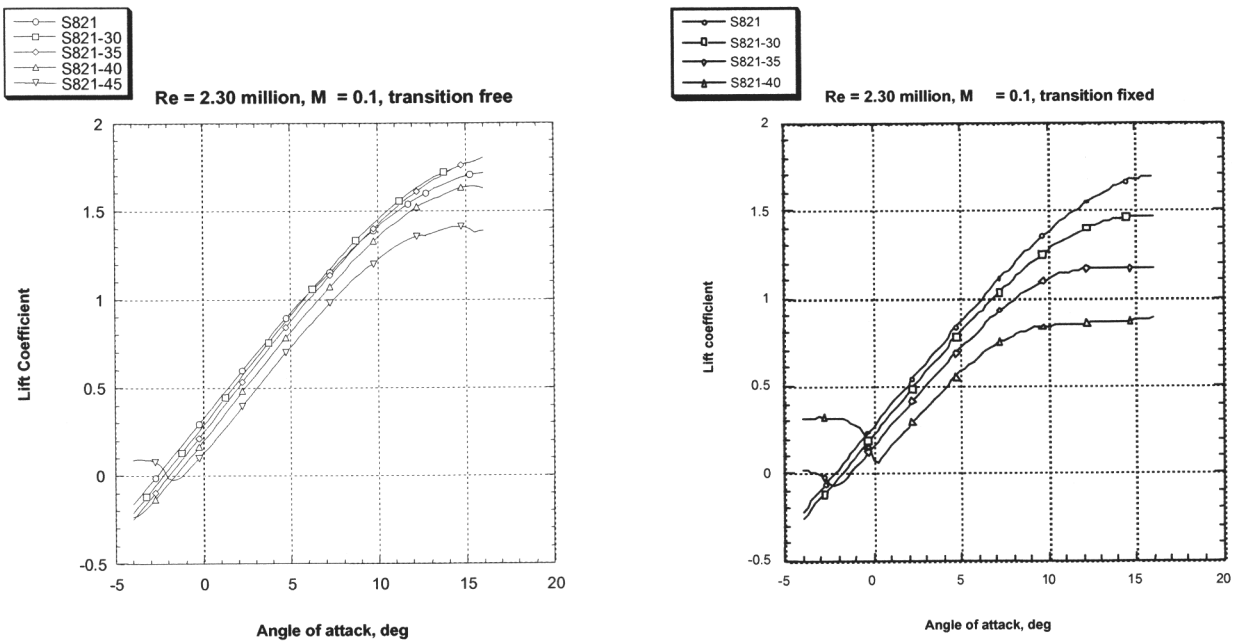

Figure 2.17 Thickness Effect on Lift at Re = 2.30 million, Free and Fixed Transition

The effect of thickness on airfoil lift-to-drag ratio is depicted in Figures 2.19 and 2.20, for free and fixed transition, and Re = 2.30 million 4.35 million, respectively. Airfoil drag increases with increasing thickness for modest lift coefficients (those less than the lift coefficient corresponding to the maximum lift-to-drag ratio).

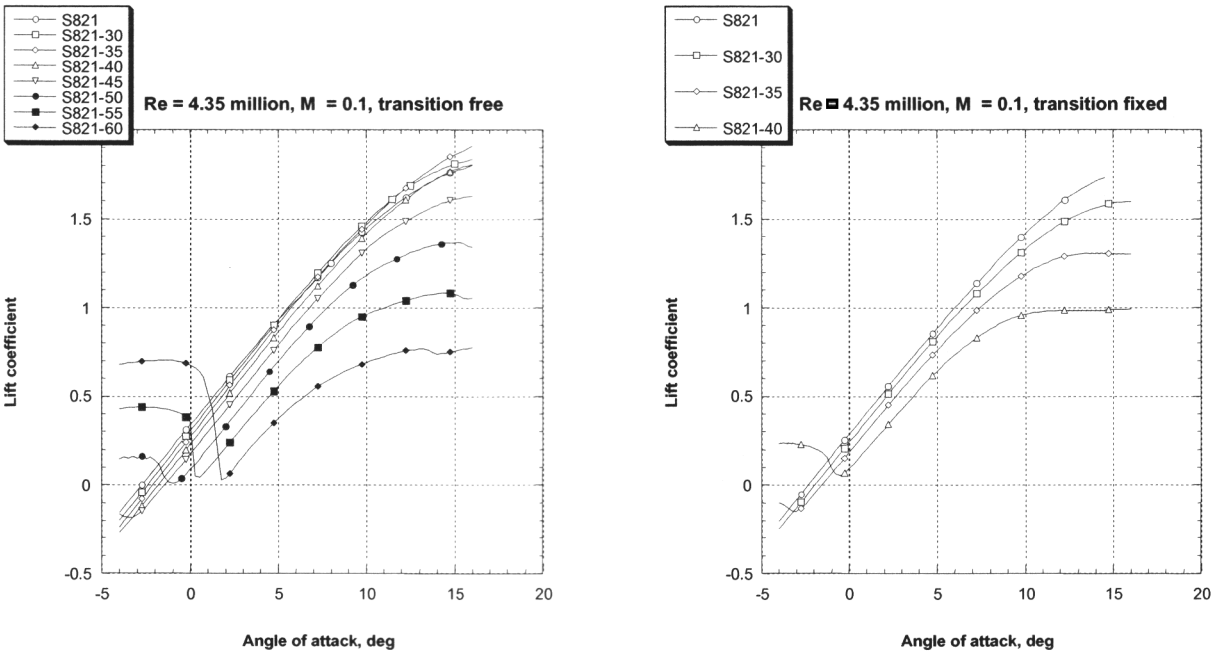

Figure 2.18 Thickness Effect on Lift at Re = 4.35 million, Free and Fixed Transition

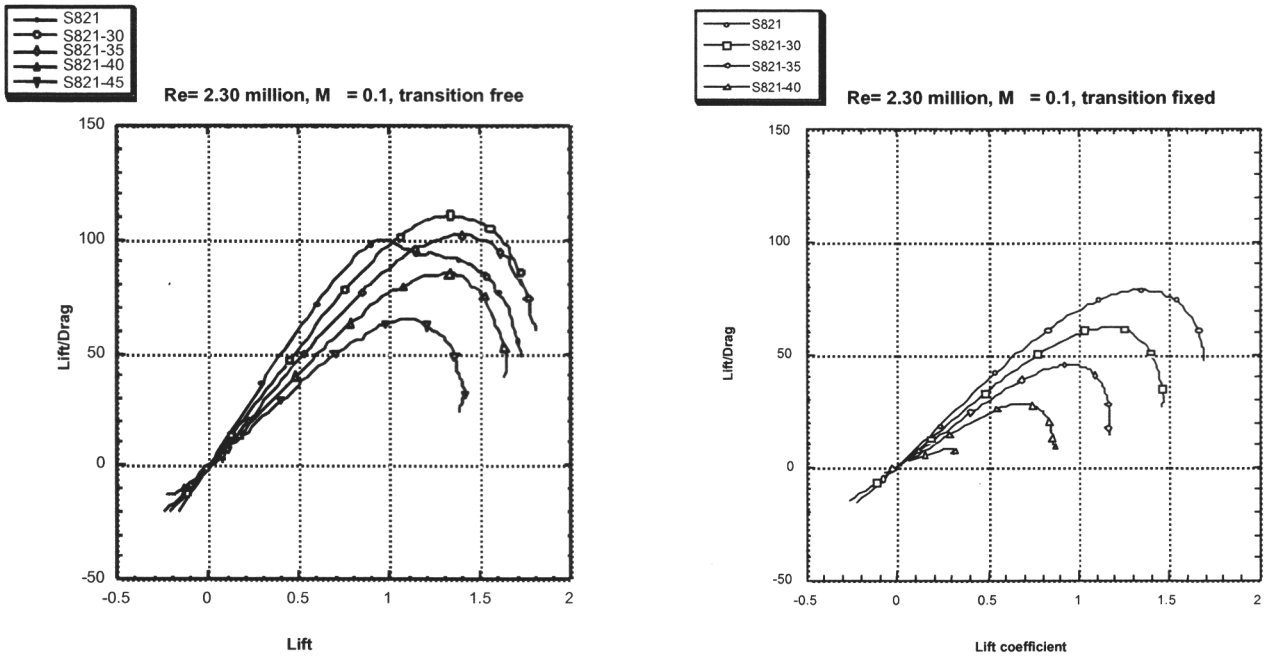

Figure 2.19 Thickness Effect on L/D at Re = 2.30 million, Free and Fixed Transition

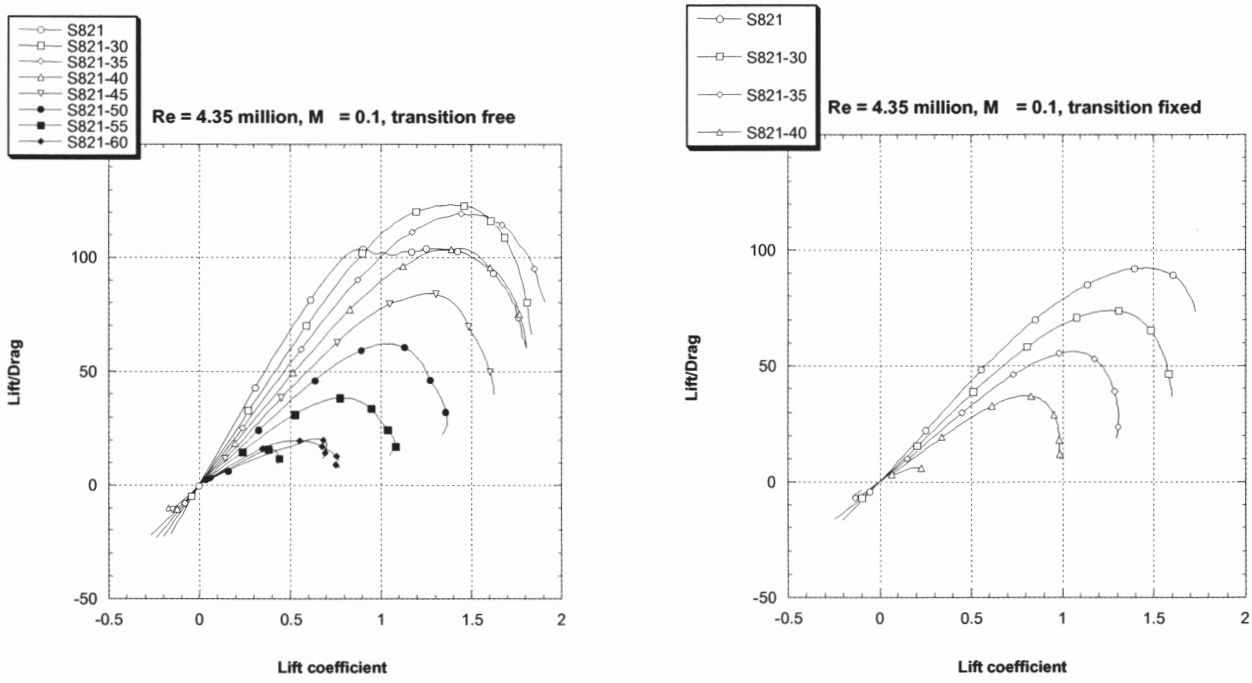

Figure 2.20 Thickness Effect on L/D at Re = 4.35 million, Free and Fixed Transition

At transition free conditions airfoil lift-to-drag ratio peaks at t/c = 0.30. However, with transition fixed near the leading edge all airfoils show a large increase in drag with the baseline airfoil performing better than the thickened airfoils. Again, redesigning the thickened airfoils and/or the addition of vortex generators on the suction surface may reduce the drag penalty due to premature transition.

2.3.2 Effect of Scaling Approach on Airfoil Performance

One problem that is often encountered in the design of wind turbine blades is aerodynamic performance of interpolated sections. Typically three to five airfoils are used as inputs to define the section shapes of a turbine blade. Through interpolation this input set is expanded by an order of magnitude to provide the section shapes that are used to manufacture the blade. The question arises how best to interpolate and what is the effect of this interpolation process on the aerodynamic performance of the generated sections. Here one example is presented to illustrate this issue. Airfoil station 25% 38%t/c is presented in Figure 2.21. This section is the result of this interpolation process. Here its aerodynamic performance characteristics are compared against those of the S821-38. This figure shows the sharp trailing-edge airfoil S821-38 and airfoil 25% 38%t/c with a trailing-edge thickness to chord ratio of 0.014.

The effect of section shape on airfoil lift predicted by MSES is depicted in Figures 2.21. The results show that straight forward XY interpolation (Station 25%, 38% t/c)changes the thickness distribution as well as the camber distribution and the lift compared to the aerodynamic scaling approach (S821-38), which maintained the mean line and airfoil camber . Maximum lift is unchanged at transition free conditions but the interpolated airfoil performance is better at transition fixed conditions. Part of this improved

performance is the result of the blunt trailing edge, as discussed in the next section. The effect of section shape on airfoil lift-to-drag ratio is depicted in Figures 2.22 and 2.23. These results show the drag characteristics to be approximately unchanged in the linear lift range.

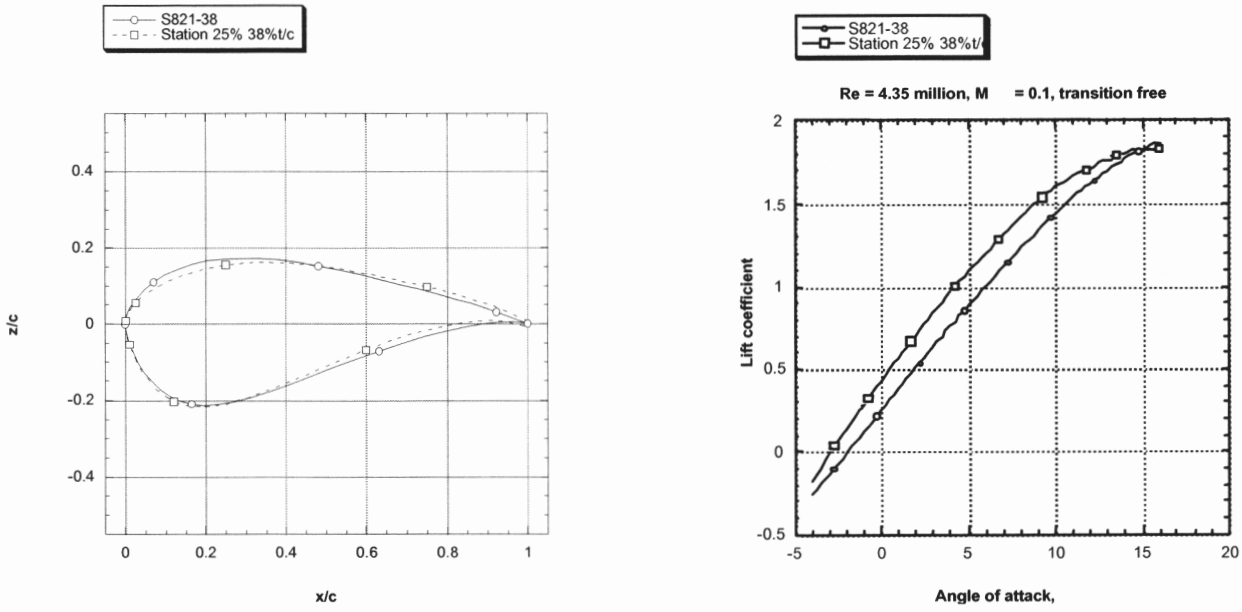

Figure 2.21 Comparison of S821-38 Airfoil and Station 25% 38% t/c Airfoil Obtained Through XY Scaling

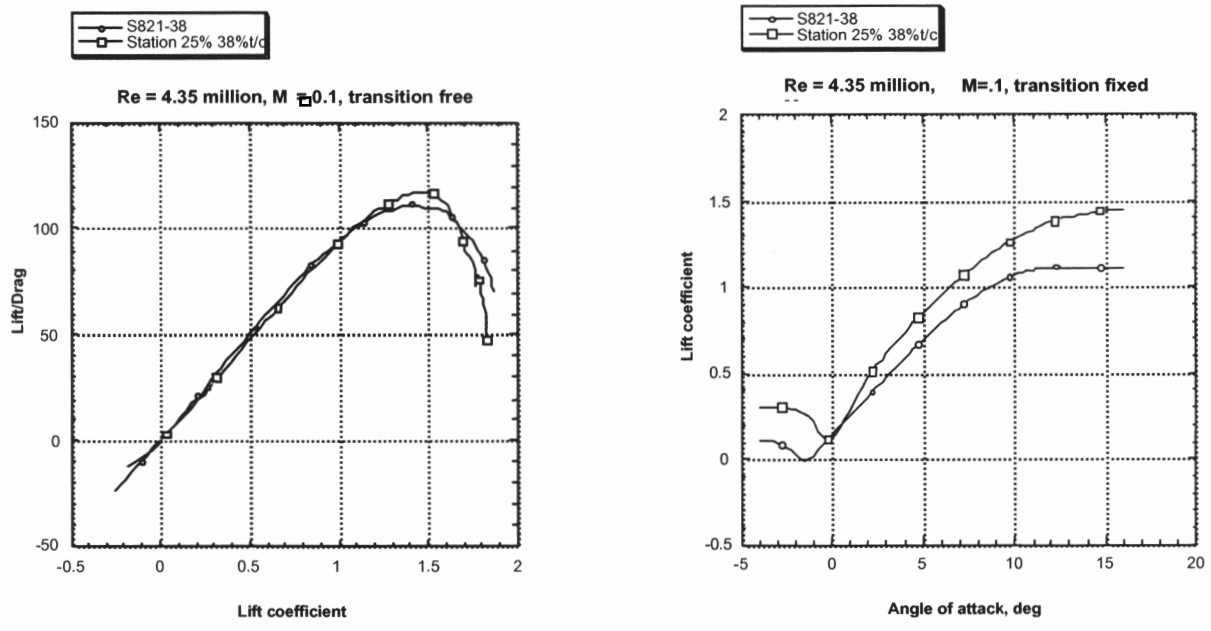

Figure 2.22 Effect of Airfoil shape on Lift and Lift-to-Drag Ratio at Re = 4.35 million, Free and Fixed Transition

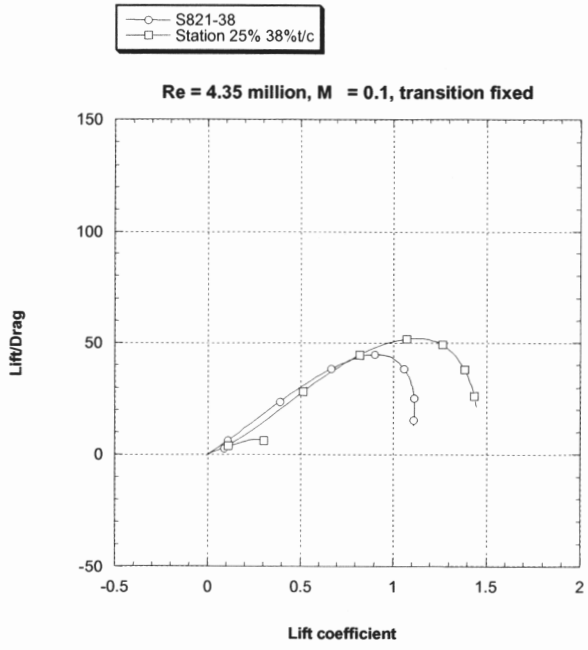

Figure 2.23 Effect of Airfoil Shape on Lift-to-Drag Ratio at Re = 4.35 million, Free and Fixed Transition

2.3.3 Effect of Trailing-Edge Thickness on Aerodynamic Performance

Aerodynamic design dictates the use of sharp trailing edges for subsonic airfoils to minimize profile drag. However, thick trailing edges reduce the amount of pressure recovery on the suction side of the airfoil and this may be especially beneficial for thick airfoils. Another advantage is that sharp trailing edges are difficult to manufacture and are easily damaged during transportation and blade installation. A limited study was conducted to evaluate the effect of trailing-edge thickness on the aerodynamic performance of the S821-38. Figure 2.23 shows the sharp trailing-edge airfoil S821-38 and the modified airfoil,S821-38-02, with a trailing-edge thickness to chord ratio of 0.02. The sharp trailing-edge airfoil was modified by adding a linear wedge (x/c = 0, t/c = 0 and x/c =1, t/c = 0.01) to the lower and upper surface. Next the airfoil's thickness distribution was altered in the same way as explained above to retain the maximum thickness-to-chord ratio of 0.38.

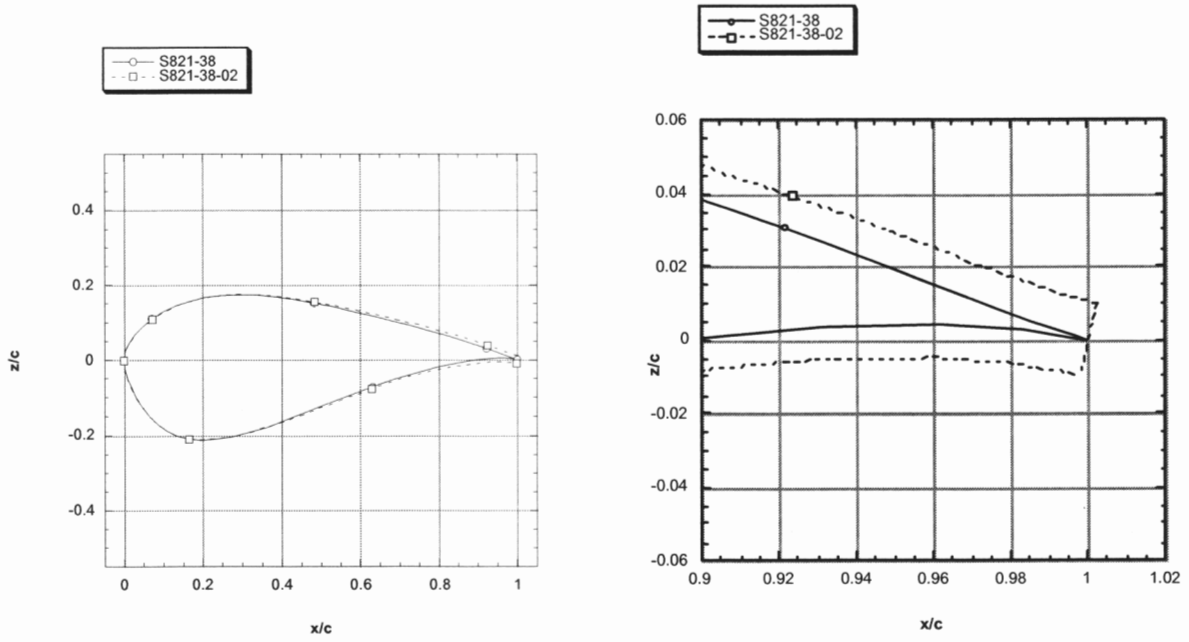

Figure 2.23 Comparison of Sharp-Trailing-Edge Airfoil S821-38 and Airfoil S821-38-02 With Trailing-Edge Thickness of 2.0%

The effect of trailing-edge thickness on airfoil lift is depicted in Figures 2.24. The results show a beneficial influence of trailing-edge thickness on the lift-curve slope as well as the maximum lift coefficient. In addition the blunt trailing edge airfoil appears to be less sensitive to loss of laminar flow. The effect of trailing-edge thickness on airfoil lift-to-drag ratio is depicted in Figures 2.25. Again, the results show a beneficial influence of trailing-edge thickness on drag for this type of thick airfoil. The effect of much thicker trailing edges on the lift and drag characteristics will be evaluated later.

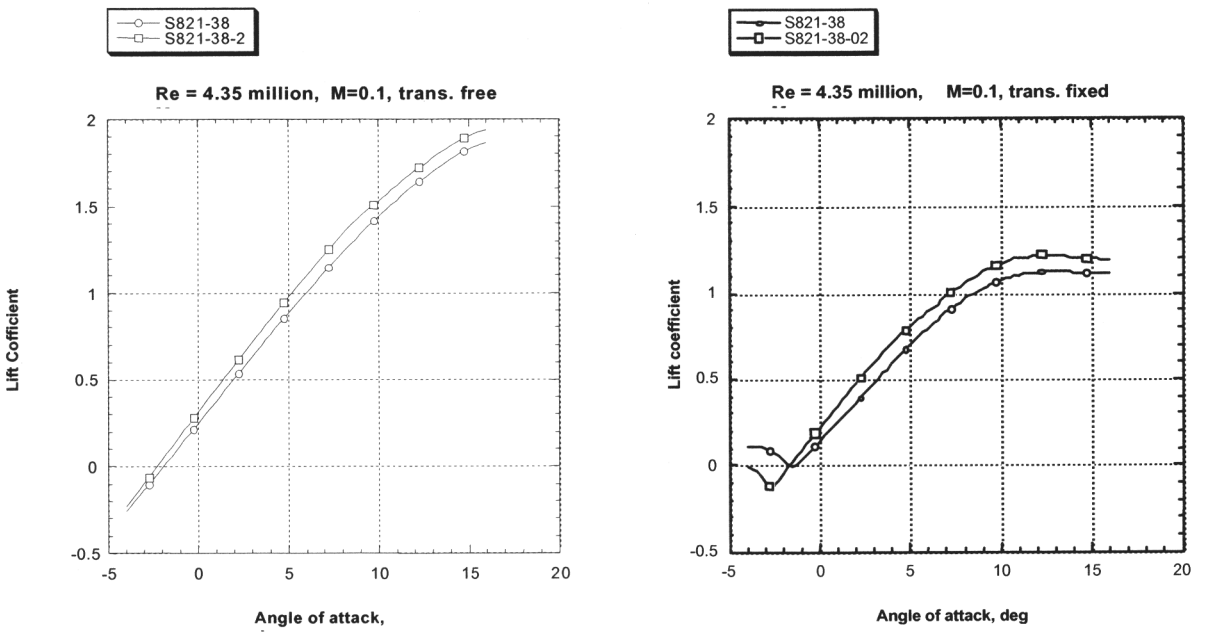

Figure 2.24 Effect of Trailing-Edge Thickness Shape on Airfoil Lift at Re = 4.35 million, Free and Fixed Transition

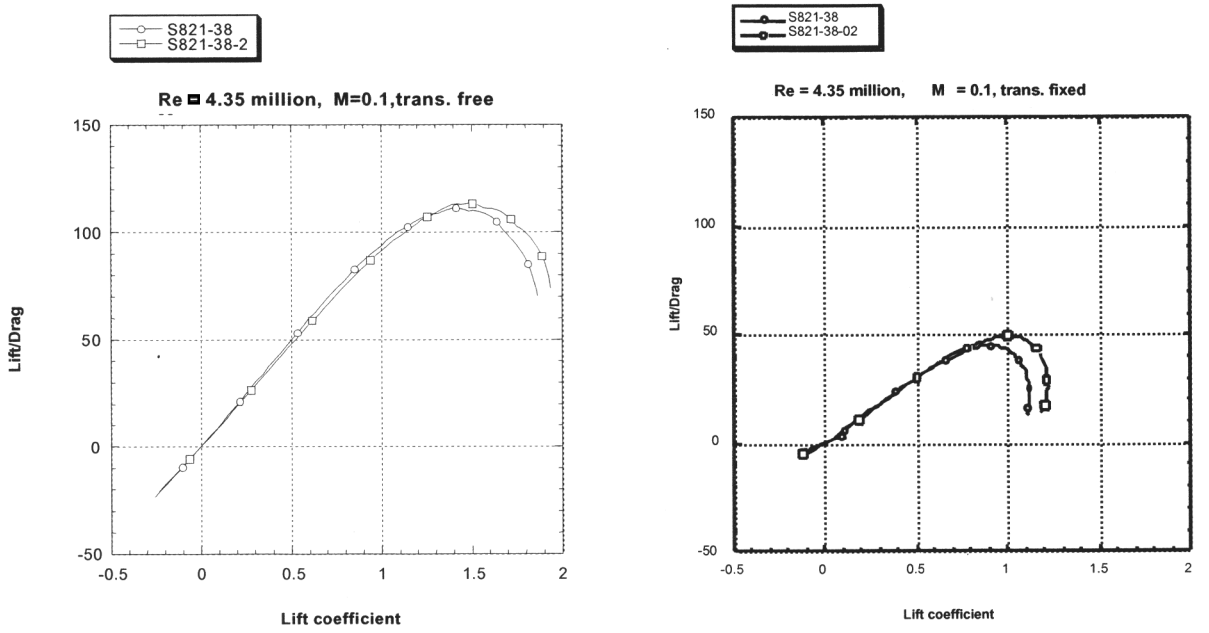

Figure 2.25 Effect of Trailing-Edge Thickness Shape on Airfoil Lift-to-Drag Ratio at Re = 4.35 million, Free and Fixed Transition

3.0 CONCLUSIONS

3.1 Significant Findings

- When going from 30 to 70 meters in blade length, the specific weight in kg/m^2 of the baseline blade more than doubled. A number of design changes will be required to limit weight, and hence, cost growth. No one technology can stop weight growth, but it can be limited by a number of design approaches.

- Increased airfoil section thickness in the inboard rotor region appears to be a key tool in limiting blade weight and cost growth with scale. From the baseline to thickest blade distribution the specific weight was reduced by 15%, due to increased structural performance.

- Larger blades may require higher tip speeds combined with reduced blade solidity to limit growth of design loads. A slender blade can be used to reduce extreme design loads when the rotor is parked, but requires a higher tip speed. Noise issues become a concern with higher tip speeds.

- Blade tip speed can strongly impact peak power. Tip speed has a weaker, but still positive influence on annual energy capture.

3.2 Recommendations for Further Study Resulting From This Study

- Increased airfoil section thickness may be a key tool in limiting blade weight and cost growth with scale. The problem with thick (t/c > 26%) airfoils is that their lift performance is sensitive to changes in the boundary layer location (i.e. the lift at fixed angle of attack decreases as a result of a forward shift in transition due to surface fouling). This sensitivity to premature transition is reduced by increasing trailing edge thickness. Thickened and truncated trailing edges in the inboard region provide strong, positive effects on blade structural performance.

    - Calculate truncated airfoil section structural properties.
    - Evaluate the aerodynamic characteristics of truncated sections.

- Increased tip speed and reduced solidity.

    - Evaluate noise issues for increased tip speed.
    - Assess performance and loads for lower solidity blades.
    - Evaluate planform shapes that raise solidity inboard and reduce it outboard.

4.0 REFERENCES

1. Blade Manufacturing Improvements: Development of the ERS-100 Blade: Project: Final Report, TPI Composites, SAND2001-1381, May 2001.

2. Zuteck, M.; "The Development and Manufacture of Wood Composite Wind Turbine Rotors", Proceedings of the Large Horizontal-Axis Wind Turbines Conference, DOE CONF-810752, SERI/CP-635-1273, July 1981.

3. Stroebel, T., Dechow, C, and Zuteck, M.; Design of Advanced Wood Composite Rotors, Gougeon Brothers, DOE/NASA/0260-1, NASA CR-174713, December 1984.

4. Zuteck, M. and Miller, M.; Hawaii Zuteck Rotor Project: Compilation of Project Reports, NREL/SR-500-26086, November 1998.

5. Abbott, I.H., and von Doenhoff, A.E., Theory of Wing Sections, McGraw Hill, 1949.

6. Tangler, J.L., and Somers, D.M., "NREL Airfoil Families for HAWTs," NREL/TP-442-7109, Jan. 1995.

7. Drela, M., "Newton Solution of Coupled Viscous/Inviscid Multielement Airfoil Flows," AIAA Paper 90-1470, June 1990.

8. Giles, M.B., and Drela, M., "Two-Dimensional Transonic Aerodynamic Design Method," AIAA Journal, Vol. 25, No. 9, Sep. 1987, pp. 1199-1206.

9. Drela, M., and Giles, M., "Viscous-Inviscid Analysis of Transonic and Low Reynolds Number Airfoils," AIAA Journal, Vol. 25, No. 10, Oct. 1987, pp.1347-1355.

DISTRIBUTION

H. Ashley
Dept. of Aeronautics and
Astronautics Mechanical Engr.
Stanford University
Stanford, CA 94305

K. Bergey
University of Oklahoma
Aero Engineering Department
Norman, OK 73069

D. Berry
TPI Composites Inc.
373 Market Street
Warren, RI 02885

R. Blakemore
GE Wind
13681 Chantico Road
Tehachapi, CA 93561

C. P. Butterfield
NREL
1617 Cole Boulevard
Golden, CO 80401

G. Bywaters
Northern Power Systems
Box 999
Waitsfield,VT 05673

J. Cadogan
Office of Wind and Hydro Technology
EE-12
U.S. Department of Energy
1000 Independence Avenue SW
Washington, DC 20585

D. Cairns
Montana State University
Mechanical & Industrial Engineering Dept.
220 Roberts Hall
Bozeman, MT 59717

S. Calvert
Office of Wind and Hydro Technology
EE-12
U.S. Department of Energy
1000 Independence Avenue SW
Washington, DC 20585

J. Chapman
OEM Development Corp.
840 Summer St.
Boston, MA 02127-1533

Kip Cheney
PS Enterprises
222 N. El Segundo, #576
Palm Springs, CA 92262

C. Christensen, Vice President
GE Wind
13681 Chantico Road
Tehachapi, CA 93561

R. N. Clark
USDA
Agricultural Research Service
P.O. Drawer 10
Bushland, TX 79012

C. Cohee
Foam Matrix, Inc.
1123 East Redondo Blvd.
Inglewood, CA 90302

J. Cohen
Princeton Economic Research, Inc.
1700 Rockville Pike
Suite 550
Rockville, MD 20852

C. Coleman
Northern Power Systems
Box 999
Waitsfield, VT 05673

K. J. Deering
The Wind Turbine Company
515 116th Avenue NE
No. 263
Bellevue, WA 98004

A. J. Eggers, Jr.
RANN, Inc.
744 San Antonio Road, Ste. 26
Palo Alto, CA 94303

D. M. Eggleston
DME Engineering
1605 W. Tennessee Ave.
Midland, TX 79701-6083

P. R. Goldman
Director
Office of Wind and Hydro Technology
EE-12
U.S. Department of Energy
1000 Independence Avenue SW
Washington, DC 20585

D. Griffin
GEC
5729 Lakeview Drive NE, Ste. 100
Kirkland, WA 98033

C. Hansen
Windward Engineering
4661 Holly Lane
Salt Lake City, UT 84117

C. Hedley
Headwaters Composites, Inc.
PO Box 1073
Three Forks, MT 59752

S. Hock
Wind Energy Program
NREL
1617 Cole Boulevard
Golden, CO 80401

D. Hodges
Georgia Institute of Technology
270 Ferst Drive
Atlanta, GA 30332

Bill Holley
3731 Oakbrook
Pleasanton, CA 94588

K. Jackson
Dynamic Design
123 C Street
Davis, CA 95616

E. Jacobsen
GE Wind
13000 Jameson Rd.
Tehachapi, CA 93561

G. James
University of Houston
Dept. of Mechanical Engineering
4800 Calhoun
Houston, TX 77204-4792

M. Kramer
Foam Matrix, Inc.
PO Box 6394
Malibu CA 90264

A. Laxson
NREL
1617 Cole Boulevard
Golden, CO 80401

S. Lockard (5)
TPI Composites Inc.
373 Market Street
Warren, RI 02885

J. Locke, Associate Professor
Wichita State University
207 Wallace Hall, Box 44
Wichita, KS 67620-0044

D. Malcolm
GEC
5729 Lakeview Drive NE, Ste. 100
Kirkland, WA 98033

J. F. Mandell
Montana State University
302 Cableigh Hall
Bozeman, MT 59717

T. McCoy
GEC
5729 Lakeview Drive NE, Ste. 100
Kirkland, WA 98033

L. McKittrick
Montana State University
Mechanical & Industrial Engineering Dept.
220 Roberts Hall
Bozeman, MT 59717

P. Migliore
NREL
1617 Cole Boulevard
Golden, CO 80401

A. Mikhail
Clipper Windpower Technology, Inc.
7985 Armas Canyon Road
Goleta, CA 93117

W. Musial
NREL
1617 Cole Boulevard
Golden, CO 80401

NWTC Library (5)
NREL
1617 Cole Boulevard
Golden, CO 80401

B. Neal
USDA
Agricultural Research Service
P.O. Drawer 10
Bushland, TX 79012

V. Nelson
Department of Physics
West Texas State University
P.O. Box 248
Canyon, TX 79016

T. Olsen
Tim Olsen Consulting
1428 S. Humboldt St.
Denver, CO 80210

R. Z. Poore, President
Global Energy Concepts, Inc.
5729 Lakeview Drive NE
Suite 100
Kirkland, WA 98033

R. G. Rajagopalan
Aerospace Engineering Department
Iowa State University
404 Town Engineering Bldg.
Ames, IA 50011

J. Richmond
MDEC
3368 Mountain Trail Ave.
Newbury Park, CA 91320

Michael Robinson
NREL
1617 Cole Boulevard
Golden, CO 80401

D. Sanchez
U.S. Dept. of Energy
Albuquerque Operations Office
P.O. Box 5400
Albuquerque, NM 87185

R. Sherwin
Atlantic Orient
PO Box 1097
Norwich, VT 05055

Brian Smith
NREL
1617 Cole Boulevard
Golden, CO 80401

J. Sommer
Molded Fiber Glass Companies/West
9400 Holly Road
Adelanto, CA 93201

K. Starcher
AEI
West Texas State University
P.O. Box 248
Canyon, TX 79016

F. S. Stoddard
79 S. Pleasant St. #2A
Amherst, MA 01002

A. Swift
University of Texas at El Paso
320 Kent Ave.
El Paso, TX 79922

J. Thompson
ATK Composite Structures
PO Box 160433
MS YC14
Clearfield, UT 84016-0433

R. W. Thresher
NREL
1617 Cole Boulevard
Golden, CO 80401

S. Tsai
Stanford University
Aeronautics & Astronautics
Durand Bldg. Room 381
Stanford, CA 94305-4035

W. A. Vachon
W. A. Vachon & Associates
P.O. Box 149
Manchester, MA 01944

C. P. van Dam
Dept of Mech and Aero Eng.
University of California, Davis
One Shields Avenue
Davis, CA 95616-5294

B. Vick
USDA, Agricultural Research Service
P.O. Drawer 10
Bushland, TX 79012

K. Wetzel
K. Wetzel & Co., Inc.
PO Box 4153
4108 Spring Hill Drive
Lawrence, KS 66046-1153

R. E. Wilson
Mechanical Engineering Dept.
Oregon State University
Corvallis, OR 97331

M. Zuteck
MDZ Consulting
601 Clear Lake Road
Clear Lake Shores, TX 77565

M.S. 0557	T. J. Baca, 9125
M.S. 0557	T. G. Carne, 9124
M.S. 0708	H. M. Dodd, 6214 (25)
M.S. 0708	T. D. Ashwill, 6214 (10)
M.S. 0708	D. E. Berg, 6214
M.S. 0708	R. R. Hill, 6214
M.S. 0708	P. L. Jones 6214
M.S. 0708	D. L. Laird, 6214
M.S. 0708	D. W. Lobitz, 6214
M.S. 0708	M. A. Rumsey, 6214
M.S. 0708	H. J. Sutherland, 6214
M.S. 0708	P. S. Veers, 6214
M.S. 0708	J. Zayas, 6214
M.S. 0847	K. E. Metzinger, 9126
M.S. 0958	M. Donnelly, 14172
M.S. 1490	A. M. Lucero, 12660
M.S. 0612	Review & Approval Desk, 9612 For DOE/OSTI
M.S. 0899	Technical Library, 9616 (2)
M.S. 9018	Central Technical Files, 8945-1